A generalized solution for transient radial flow in hierarchical multifractal fractured aquifers

Gerard Lods, Philippe Gouze

A generalized solution for transient radial flow in hierarchical multifractal fractured aquifers

Gérard Lods[1] and Philippe Gouze[1]

Received 30 April 2008; revised 3 September 2008; accepted 17 September 2008; published 5 December 2008.

[1] An analytical solution in the Laplace domain is derived for modeling anomalous pressure diffusion during pumping tests in aquifer displaying hierarchical fractal fracture networks. The proposed solution generalizes all of the analytical models for fractal flow published previously by combining multifractal diffusion and nested multiporosity with transient exchanges, interface skin effects, and well storage effect. Solutions are derived for fracture-delimited blocks with planar, cylindrical, and spherical shapes, as well as with any fractional dimensional shapes. Any combinations of these shapes can be defined in order to model a large range of situations. Within each permeability level, the fractal properties of the fracture network can be specified and the fractal dimension can be distinct from the shape dimension of the block.

Citation: Lods, G., and P. Gouze (2008), A generalized solution for transient radial flow in hierarchical multifractal fractured aquifers, *Water Resour. Res.*, *44*, W12405, doi:10.1029/2008WR007125.

1. Introduction

[2] Hydraulic properties of reservoirs are usually inferred from well tests (either pumping or injection tests) by fitting the parameters of heuristic models that account for the assumed hydrodynamic features (e.g., heterogeneity) of the medium. For instance, fractured reservoirs often display distinct sets of conductive fractures which may be connected to each other, and which usually delimit less conductive zones. In their pioneering work, *Barenblatt et al.* [1960] introduced the double-porosity concept, proposing that reservoirs can be represented by two overlapping continua with distinctly different porosity values. They distinguished a main fracture network, where flow takes place at the scale of the volume affected by the pumping test, and porous blocks that can be drained by the fractures. Mass transfers between fractures and blocks can be modeled either by stationary [*Warren and Root*, 1963] or transient [*Boulton and Streltsova*, 1977] formulations. Stationary exchange models assume instantaneous diffusion in the blocks, while the mass exchange rate is controlled by the difference in head between the fracture and the block. The transient exchange approach is much more realistic, and has been improved by parameterization of the fracture skin effect [*Moench*, 1984] that allows modeling of the expected hydraulic impedance at the fracture-block interface due to the presence of pre-existing mineral deposits or an alteration layer. The introduction of the skin effect unifies the two types of exchange, since fracture-block exchange tends to be stationary if fracture-block impedance is high.

[3] Several models have been proposed to account for more complex reservoir properties and specific shapes of the drawdown or recovery curves derived from pumping tests. The triple-porosity model was introduced by *Closman* [1975], and further developed by *Abdassah and Ershaghi* [1986], who proposed analytical solutions to model flow in a fractured network exchanging water (transient) with two matrix continua displaying distinct hydrodynamic properties. *Rodriguez et al.* [2004] proposed analytical solutions with stationary exchanges between two nested sets of fractures and a porous matrix. *Pulido et al.* [2006] addressed solutions for modeling transient exchanges, including the skin effect, between a fracture network, a microfracture network and a porous matrix assuming that microfractures are unconnected on a large scale.

[4] The presence of vugular cavities in reservoirs has also been investigated. *Liu et al.* [2003] proposed analytical solutions with stationary exchange between a fracture network, vugular cavities and matrix blocks, assuming that vugular cavities are unconnected at the large scale (i.e., fractures segregate both the matrix and the vugular cavities). This model was extended to the possible large-scale connectivity of vugular cavities (i.e., vugular cavities are connected to the well) by *Camacho-Velázquez et al.* [2005], while *Pulido et al.* [2007] gave solutions accounting for transient exchanges and skin effect between fractures, vugular cavities and matrix.

[5] A more general multicontinuum approach was proposed by *Bai et al.* [1993]. However, although multicontinuum models may be appropriate for studying fluid flow in systems with hierarchized permeability, they do not account for the fractal properties of fracture networks as commonly observed in natural reservoirs [*Le Borgne et al.*, 2004; *Bernard et al.*, 2006]. For example, the models listed above do not account for (1) the scale dependence of porosity and permeability and (2) the nonuniform connectivity distribution of fracture networks and the presence of critical links acting as bottlenecks that may generate anomalous diffusion [see *de Dreuzy and Davy*, 2007, and references herein].

[6] Fractal properties of fractured reservoirs have been studied intensively following the pioneering developments

[1]Laboratoire Géosciences, Université Montpellier 2 - CNRS, Montpellier, France.

0043-1397/08/2008WR007125

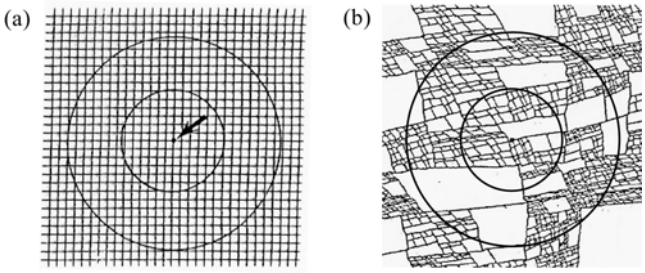

Figure 1. Synthetic two-dimensional networks with porosity and conductivity power law radial scaling, modified from the work of *Acuna and Yortsos* [1995]. (a) Uniform regular network; scaling exponents are 0. (b) Fractal distribution; negative, distinct scaling exponents of porosity and conductivity.

by *Mandelbrot* [1983]. Fragmentation processes were related to fractal properties by *Turcotte* [1986], and numerous field measurements have shown that natural fracture networks possess fractal properties [e.g., *Barton and Hsieh*, 1989; *Nolte et al.*, 1989; *Chelidze and Gueguen*, 1990; *Sahimi et al.*, 1993]. The calculation of radial diffusion in synthetic fractal networks has revealed some specific features, such as power law scaling of porosity and conductivity with the radial distance from the source, which leads to anomalous diffusion [*O'Shaughnessy and Procaccia*, 1985]. For example, Figure 1 shows a fractal two-dimensional network with porosity and conductivity scaling according to a power law with the radial distance to the centre. The fractal distribution has porosity and conductivity power law exponents of -0.22 and -0.29, respectively, while the exponents are nil in the case of a uniform network occupying the whole grid.

[7] *Barker* [1988] has proposed analytical solutions for modeling pumping tests without anomalous diffusion in a single-porosity system, but characterized by a fractional flow dimension. This model generalizes the Euclidean dimension to nonintegral flow dimensions that accounts for the fractal structure of the fracture network. The value of flow dimension is unity for a parallel flow, such as flow in a vertical fault intercepted by the pumping well. Flow dimension is 2 for cylindrical flow in a pumping test, for example, when the well completely penetrates a homogeneous porous aquifer; this is the underlying assumption of Theis's model [*Theis*, 1935]. Flow dimension is 3 for spherical flow as expected in the case of pumping concentrated within a single fracture (using a dual packer system) connected to a dense and extended network. Note however that the fractal scale dependence is restricted to identical exponents for porosity and conductivity power law in the Barker's model [*Walker and Roberts*, 2003]. Barker's model has been extended by *Hamm and Bidaux* [1996] to double-porosity systems with transient exchanges including fracture skin parameterization. Models with a fractional flow dimension have proved useful in cases where integral dimension solutions are not satisfactory [*Lods and Gouze*, 2004], but they do not account for anomalous diffusion. Analytical solutions for anomalous diffusion have been put forward by *Chang and Yortsos* [1990], generalizing the single-porosity model of *Barker* [1988].

[8] The aim of the present study is to provide analytical solutions for modeling anomalous pressure diffusion during pumping tests in aquifer displaying hierarchical fractal fractures sets. The proposed solutions generalize all the models presented above (see Table 1). We consider a main fracture network intercepted by the pumping well. This fracture network delimits blocks in which fractal diffusion is controlled by fractures at a lower level (Figure 2). This hierarchy is implemented recursively, which eventually leads to a hierarchical fractal permeability system (or multifractal system). Each of the fracture levels exchanges water with the blocks that are delimited in this way. Exchanges are transient and take into account possible skin effects. Solutions are derived for a block shape of dimension 1 for planar blocks, 2 for cylindrical blocks, and 3 for spherical blocks [*Boulton and Streltsova*, 1977; *Moench*, 1984; *Barker*, 1985a, 1985b], as well as for any fractional dimension. Any combination of these shapes is allowed. Within each permeability level, the fractal properties of the fracture network can be specified and the fractal dimension can be different from the shape dimension of the block.

[9] In addition to the skin effect that may occur at the fracture-block interfaces, our model also takes account of the wellbore skin effect [*van Everdingen*, 1953]. This effect is known to be potentially important, and is modeled here as a singular head loss or gain at the well-reservoir interface. A positive skin effect factor is used to model laminar and turbulent head losses occurring in the well, in the equipment (e.g., slotted tubing, gravel pack) or in close proximity to the well due to eventual damage during drilling operations (e.g., rock alteration or mud invasion). On the contrary, negative skin factors must be used to account for the increase in conductivity observed after well development or when the aperture of the fractures intersecting the well is large in the vicinity of the well.

[10] In addition, our model includes a parameterization of the well storage effect [*Papadopulos and Cooper*, 1967] due to the difference in storage and conductivity between the well and the reservoir. Well storage effects are particularly important for large-diameter wells and when the rock

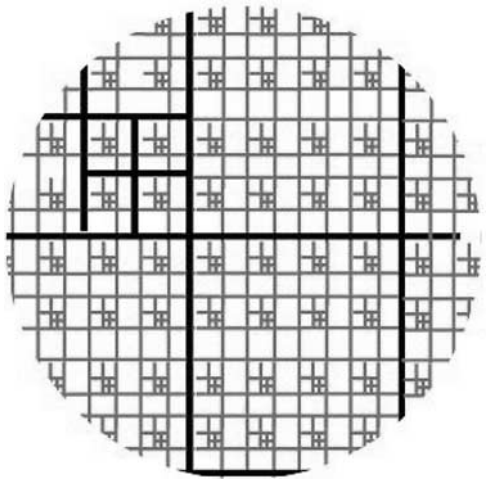

Figure 2. Schematic representation for two fracture levels. Fractures of the first domain (thick lines) make up the porosity domain P_1 and delimit blocks (by volume complementation) that are drained via the embedded fracture network (thin lines) forming the second porosity domain P_2.

Table 1. Comparison of Models[a]

	Porosity Domain 1		Porosity Domain 2				Porosity Domains $i > 2$			
	(a)	(b)	(a)	(b)	(c)	(d)	(a)	(b)	(c)	(d)
Barker [1988]	yes	no	-	-	-	-	-	-	-	-
Chang and Yortsos [1990]	yes	yes	-	-	-	-	-	-	-	-
Hamm and Bidaux [1996]	yes	no	no	no	yes	no	-	-	-	-
This paper	yes	yes	yes	yes	yes	yes	yes	yes	yes	yes

[a]Analytical solutions accounting for fractal properties: (a) fractional flow dimension, (b) anomalous diffusion, (c) fracture skin, (d) fractional block shape dimension.

formation conductivity is low. Note that this effect cannot be taken into account in models assuming an infinitesimal source, such as in Theis's model.

[11] In the next section, we present the governing equations and solutions in the Laplace domain (the full mathematical treatments are given in Appendix A). The application and parameterization of the model is discussed and illustrated in section 3, along with examples of increasing complexity as well as a parameter sensitivity analysis. Section 4 provides some concluding remarks emphasizing the improvements and some limitations of the model.

2. Governing Equations

[12] In the following, we assume a confined isotropic aquifer, radially infinite and initially at rest. Flow occurs in a hierarchical fractured system containing m levels of fractures. The first fracture network level is fully connected within the entire domain, and consequently to the pumping well. This fracture network forms the porosity domain P_1 and delimits blocks defined by volume complementation. The blocks within P_1 are fractured by fractures that form the porosity domain P_2. The porosity domain P_2 is not fully connected since it is segregated by the fractures forming the porosity domain P_1, but the properties of P_2 are assumed to be statistically identical in each of the blocks. The same hierarchical organization is applied recursively for $i = 2, \ldots, m - 2$, where porosity domain P_i is made up of fractures delimiting blocks that are drained peripherally. These blocks are affected by fractures forming the fracture network of level $i + 1$ (i.e., the porosity domain P_{i+1}). The porosity domain P_{m-1} delimits the smallest permeable blocks (the porosity domain P_m) and drains them peripherally. The properties are assumed statistically identical in each of the segregated blocks embedding the porosity domain P_i for $2 < i \leq m$. By convention, the blocks embedding domain P_i are referred to in the following as P_i blocks.

[13] To account for fractal flow, *Acuna and Yortsos* [1995] proposed that hydraulic properties (i.e., porosity and permeability) should be set as homogeneous or scaling with the radial coordinate in each porosity domain. The first domain P_1 is formed of the most extensive fractures and is inserted in the Euclidean limit of dimension n_1, which can be regarded as a single block occupying the entire system. Domain P_1 is drained radially by a diffusion source, corresponding to the pumping chamber, which can represent the entire saturated part of the well, or alternatively a part of the well if the pumping chamber is delimited by one or two packers. For domains $P_{i>1}$, the block shape has an inner symmetry centre of dimension $3 - n_i$. Values of 1, 2 and 3 for n_i (Figures 3 and 4) correspond to planar, cylindrical and spherical shapes, respectively. We generalize this approach for nonintegral values of n_i. Consequently, any combination of block shape can be investigated. For each block, using the standard assumption of uniform peripheral pressure stress, flow is radial and the symmetry centre acts as a no-flow boundary.

2.1. Diffusion Equations and Fractal Properties

[14] In each domain P_i, the drawdown h_i [m] satisfies the differential mass balance equation with standard approximations for a slightly compressible fluid:

$$S_{sfi}(r_i)\frac{\partial h_i}{\partial t} = \frac{1}{r_i^{n_i-1}}\frac{\partial}{\partial r_i}\left(r_i^{n_i-1}K_{fi}(r_i)\frac{\partial h_i}{\partial r_i}\right) + q_{fi}, \qquad (1)$$

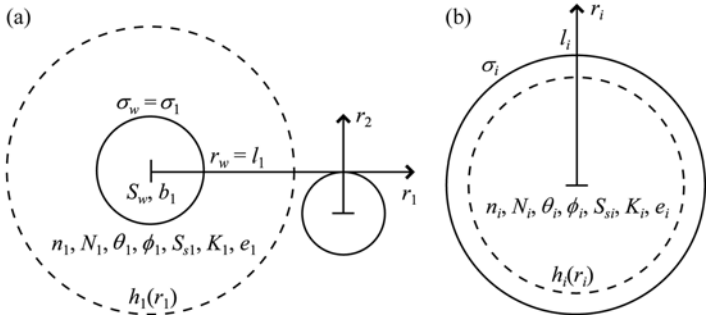

Figure 3. Orthoradial projection scheme. (a) Left figure schematizes the first domain with a finite source and one block of the second domain. (b) Right figure schematizes one block of domains $i \geq 2$. Dashed circle indicates equipotential of radius r_i. Parameters characterizing each domain are reported. Note that e_m is not used for domain m.

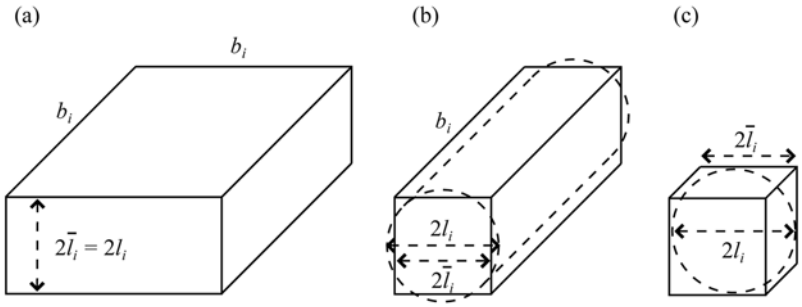

Figure 4. Truncated hyperspherical blocks (dashed) of domains $i \geq 2$, with their hypercubic equivalent for integral dimensions (a) $n_i = 1$, (b) $n_i = 2$, (c) $n_i = 3$. b_i is the orthoradial truncation length.

where r_i [m] is the radial Euclidean distance from the source centre for $P_{i=1}$, and the radial Euclidean distance from the centre of the embedding blocks for the other domains $P_{i>1}$ (Figure 3), t [s] is the elapsed time, S_{sfi} [m^{-1}] is the specific storage, K_{fi} [m s^{-1}] is the hydraulic conductivity and q_{fi} [s^{-1}] is the exchange flow rate density between P_i and P_{i+1}. By construction, $q_{fm} = 0$. Following the approach by *Acuna and Yortsos* [1995], we can define the fractal scaled values (denoted by *f* subscript) for specific storage S_{sfi} and hydraulic conductivity K_{fi} as follows:

$$K_{fi}(r_i) = K_i r_i^{N_i - n_i - \theta_i}, \tag{2}$$

and:

$$S_{sfi}(r_i) = S_{si} r_i^{N_i - n_i}, \tag{3}$$

where S_{si} and K_i are the values of the specific storage and the hydraulic conductivity on the unit radius hypersphere. Similarly, this scaling can be applied for porosity:

$$\phi_{fi}(r_i) = \phi_i r_i^{N_i - n_i} \tag{4}$$

where ϕ_i is the porosity value on the unit-radius hypersphere. In this study, we implement the standard relations (as used in petroleum engineering, for example) between S_{si}, K_i and ϕ_i: $S_{si} = \bar{\rho}\phi_i c_i$ and $K_i = \bar{\rho}\phi_i k_i/\mu$, where $\bar{\rho}$ [kg m^{-2} s^{-2}] denotes the product of the fluid density and the gravity acceleration, μ [m^{-1} s^{-1} kg] is the dynamic viscosity of the fluid, c_i [m s^2 kg^{-1}] is the total compressibility and k_i [$m^{2+\theta_i}$] is the fractal permeability. In equations (2) to (4), N_i is the (fractal) density dimension of the fracture network ($N_i \leq n_i$) and θ_i is the anomalous diffusion exponent ($\theta_i \geq 0$). Anomalous diffusion arises, for example, from null-aperture distributed zones in individual fractures or from pore-space connectivity of the fracture network [*de Dreuzy and Davy*, 2007]. The anomalous diffusion exponent is related to the random walk dimension θ'_i on a fractal lattice, by $\theta_i = 2 - \theta'_i$ [*Havlin and Ben-Avraham*, 1987]. Conversely, the fractal density dimension N_i is related to the spectral dimension N'_i ($1 \leq N'_i \leq N_i$), which corresponds to the flow dimension of Barker's model [*Barker*, 1988]:

$$N'_i = 2N_i/(2 + \theta_i). \tag{5}$$

Initial and boundary conditions are defined by:

$$h_i(t = 0) = 0, \tag{6}$$

$$\lim_{r_1 \to \infty} h_1 = 0, \tag{7}$$

and

$$\lim_{r_i \to 0} \left[K_{fi} \frac{\partial h_i}{\partial r_i} \right] = 0, \qquad i > 1. \tag{8}$$

2.2. Exchange Terms

[15] The exchange flow rate density q_{fi} is the product of the exchange area density and the local velocity. Assuming that the hydraulic conductivities of domain P_i and P_{i+1} are distinctly different, the local velocity is controlled by the conductivity value of the less conductive porosity domain. Then, taking $K_{fi+1} < K_{fi}$ by construction, we obtain the exchange flow rate density, q_{fi}, for porosity domains $P_{i<m}$:

$$q_{fi} = -\chi_{fi+1} \left(K_{fi+1} \frac{\partial h_{i+1}}{\partial r_{i+1}} \right)_{r_{i+1} = l_{i+1}}, \tag{9}$$

where χ_{fi+1} [m^{-1}] is the exchange area density, and l_{i+1} is the hyperspherical block radius of domain $P_{i+1>1}$. The exchange areas are equipotentials that have a hyperspherical symmetry (generalization of spherical symmetry to an arbitrary dimension). However, fractured media are usually modeled by suborthogonal fractures that form planar, parallelepipedal or cubic blocks [*Boulton and Streltsova*, 1977; *Moench*, 1984; *Barker*, 1985a, 1985b]. We generalize here the block shape to account for hypercubic symmetry, i.e., the generalization of cubic symmetry to an arbitrary dimension (Figure 4). To maintain geometrical coherence between hypercubes and hyperspheres, we can either conserve the volume or the peripheral area, so these two possibilities are considered in the following. The shape factor β_i is defined as the ratio of the half thickness of the equivalent hypercubic block $\bar{l}_i$ [m] to the hyperspherical block radius l_i [m]. We consider here that the ratio of fracture exchange area to fracture volume is the same as in the equivalent hypercubic block distribution. By definition, for each domain P_i, χ_{fi+1} is the total exchange area with the domain P_{i+1} in a unit volume of the medium, while the porosity ϕ_{fi} is the total volume of the fractures in a unit

Table 2. Geometric Properties of the Truncated Blocks (Figures 4 and 5) Containing the Porosity Domain i ($i \geq 2$)[a]

	Density (m^{-3})	Exchange Area (m^2)		Volume (m^3)	
	D_i (cubic)	A_{iS} (spherical)	A_{iC} (cubic)	V_{iS} (spherical)	V_{iC} (cubic)
$n_i = 1$	$[(2\bar{l}_i + e_{i-1})b_i^2]^{-1}$	$2b_i^2$	$2b_i^2$	$(2l_i)\ b_i^2$	$(2\bar{l}_i)b_i^2$
$n_i = 2$	$[(2\bar{l}_i + e_{i-1})^2\ b_i]^{-1}$	$2\pi l_i\ b_i$	$4(2\bar{l}_i)b_i$	$\pi l_i^2\ b_i$	$(2\bar{l}_i)^2\ b_i$
$n_i = 3$	$[(2\bar{l}_i + e_{i-1})^3]^{-1}$	$4\pi\ l_i^2$	$6(2\bar{l}_i)^2$	$(4/3)\pi l_i^{\ 3}$	$(2\bar{l}_i)^3$
n_i fractional	$[(2\bar{l}_i + e_{i-1})^{n_i}\ b_i^{3-n_i}]^{-1}$	$G_{n_i}(b_i)l_i^{n_i-1}$	$2n_i\ (2\bar{l}_i)^{n_i-1}\ b_i^{3-n_i}$	$G_{n_i}(b_i)l_i^{n_i}/n_i$	$(2\bar{l}_i)^{n_i}\ b_i^{3-n_i}$
Shape factor $\beta_i = \bar{l}_i/l_i$ [−]		$A_{iS} = A_{iC} : \beta_i = \left(\frac{\alpha_{n_i}}{2^{n_i} n_i}\right)^{\frac{1}{n_i - 1}}$		$V_{iS} = V_{iC} : \beta_i = \left(\frac{\alpha_{n_i}}{2^{n_i} n_i}\right)^{\frac{1}{n_i}}$	
Density		$\Lambda_i = A_{iS}D_i = \frac{\alpha_{n_i}}{l_i\left(2\beta_i + \frac{e_{i-1}}{l_i}\right)^{n_i}}\ [m^{-1}]$		$\Delta_i = V_{iS}D_i = \frac{\alpha_{n_i}}{n_i\left(2\beta_i + \frac{e_{i-1}}{l_i}\right)^{n_i}}\ [-]$	

[a] $G_n(b) = \alpha_n b^{3\ -\ n}$ is the area of the unit-radius hyperspherical block of dimension n, with $\alpha_n = 2\pi^{n/2}/\Gamma(n/2)$, and Γ is the gamma function.

volume of the medium. Consequently, the ratio of fracture exchange area to fracture volume can be written as:

$$\frac{\chi_{fi+1}}{\phi_{fi}(r_i)} = \frac{\Lambda_{i+1}}{1 - \Delta_{i+1}}, \tag{10}$$

where Λ_i [m^{-1}] and Δ_i [−] denote the exchange area density and the volume density, respectively, of the P_i blocks for an hypercubic block distribution. $\Lambda_{i+1}/(1 - \Delta_{i+1})$ is the exchange area between domains P_i and P_{i+1} divided by the fracture volume of domain P_i. This relation is valid because, by volumetric complementation, $1 - \Delta_{i+1}$ is the fracture volume density of P_i.

[16] The exchange area density χ_{fi+1} defined by equation (10) scales radially, as expected for an area embedding a fractal volume that scales with the radial distance. This scaling of the exchange area density with the exponent of the porosity is in agreement with the findings by *Delay et al.* [2007], who observed a similar scaling property of the exchange coefficient with porosity. Their results were based on the analysis of pumping tests using a fractal double-porosity model with stationary exchange. This scaling accounts for the fact that, when porosity of domain P_i decreases, the exchange area density decreases because of the radius increase of the P_{i+1} block.

[17] The calculation of β_i, Λ_i and Δ_i is given in Table 2. Λ_i is defined as the product of the elementary exchange area (i.e., the exchange area of each block) and the number of blocks per unit volume (i.e., the block density). The density of P_i blocks is a function of fracture aperture e_{i-1} [m] of domains P_{i-1} with $i \geq 2$ (Figures 3 and 5). Similarly, Δ_i is defined as the product of the elementary volume (i.e., the volume of each block) and the block density. If blocks have at least one infinite dimension (i.e., for $n_i = 1$ or 2), it is not possible to calculate the exchange area and volume of a single block. Hence the values of Λ_i and Δ_i are calculated on an equivalent system of blocks, obtained by truncation of the infinite blocks into finite blocks (Figure 4). Table 2 presents the calculated values, for integral and fractional dimensions, of the truncated block density D_i [m^{-3}], the elementary exchange area A_{iS} and A_{iC} [m^2], and the elementary volume V_{iS} and V_{iC} [m^3], with S and C subscripts denoting hyperspherical and hypercubic shapes, respectively. Values of β_i are given for both cases of identity of exchange area ($A_{iS} = A_{iC}$) and volume ($V_{iS} = V_{iC}$). The formulation of Λ_i and Δ_i is given as a function of l_i and β_i.

2.3. Fracture Skin

[18] The hydraulic impedance of a mineral deposit or alteration layer occurring on the fracture walls of domain $P_{i<m}$ can be modeled as a singular head loss characterized by the dimensionless fracture skin factor coefficient σ_{i+1}. In this case, we obtain:

$$h_i = \left(h_{i+1} + l_{i+1}\sigma_{i+1}\frac{\partial h_{i+1}}{\partial r_{i+1}}\right)_{r_{i+1}=l_{i+1}}. \tag{11}$$

2.4. Pumping Well

[19] Exchange between the pumping well and the aquifer is restricted to the higher conductivity domain, i.e., domain P_1. The well mass balance differential equation is as follows:

$$S_w\frac{\partial h_w}{\partial t} = G_{n_1}(b_1)r_w^{n_1-1}\left(K_{f1}\frac{\partial h_1}{\partial r_1}\right)_{r_1=r_w} + Q, \tag{12}$$

where h_w [m] is the well drawdown, Q [$m^3\ s^{-1}$] is the injection flow rate, S_w [m^2] is the well capacity and r_w [m] is the well radius in the zone of exchange with the aquifer. For convenience, we define the characteristic length l_1 [m] of the first domain P_1 as equal to the well exchange radius r_w. The pumping chamber exchange area is represented by an equipotential with a hyperspherical symmetry. The parameter b_1 [m] is the orthoradial length of the pumping

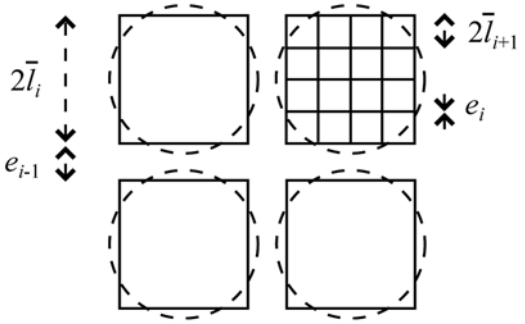

Figure 5. Orthoradial projection scheme for $n_i = 2$, showing four volume-equivalent hypercubic and hyperspherical (dashed) blocks. The fractures of the porosity domain i delimit blocks that contain the fractures forming the porosity domain $i + 1$.

chamber, that is to say, the conductive thickness in dimension 2. $G_{n_1}(b_1)$ is the area of a unit-radius hyperspherical pumping chamber of dimension n_1 and orthoradial length b_1 (see Table 2). The well-skin effect is represented by a singular head loss, using the dimensionless well skin factor σ_w, which is also denoted as σ_1 for convenience. The formulation is similar to equation (11) and can be written as:

$$h_w = \left(h_1 - r_w \sigma_w \frac{\partial h_1}{\partial r_1} \right)_{r_1 = r_w}. \tag{13}$$

If a nonlinear skin effect occurs due to turbulent flow, the value of the skin factor increases with the flow rate. We introduce a value for critical flow rate Q_c [$m^3\ s^{-1}$; $Q_c > 0$], delimiting laminar and turbulent flow, such that the Q derivative of σ_w is continuous [*Lods and Gouze*, 2004]:

$$\sigma_w = \sigma_{w\ell} + \sigma_{wt} \mathrm{H}(|Q| - Q_c)(|Q| - Q_c)^{p_w}/|Q|, \tag{14}$$

where $\sigma_{w\ell}$ [−] and σ_{wt} [$m^{3(1\ -\ p_w)}\ s^{p_w - 1}$] are the linear (laminar) and nonlinear (turbulent) skin factor coefficients, respectively, setting $\sigma_{wt} > 0$, while p_w [−] is the nonlinear head loss exponent [*Rorabaugh*, 1953], with $p_w > 1$, and H is the Heaviside function. The initial condition is defined by:

$$h_w(t = 0) = 0. \tag{15}$$

2.5. Scaling Law Substitution

[20] By substituting the scaling laws (equations (2) to (4)) in equations (1), (9), (10), and (12), we obtain diffusion equations having the same constant parameters as those defined on the unit-radius hypersphere:

$$S_{si} \frac{\partial h_i}{\partial t} = \frac{1}{r_i^{N_i - 1}} \frac{\partial}{\partial r_i} \left(r_i^{N_i - 1 - \theta_i} K_i \frac{\partial h_i}{\partial r_i} \right) + q_i, \tag{16}$$

$$q_m = 0, \tag{17}$$

$$q_i = -\chi_{i+1} l_{i+1}^{N_{i+1} - n_{i+1} - \theta_{i+1}} K_{i+1} \left(\frac{\partial h_{i+1}}{\partial r_{i+1}} \right)_{r_{i+1} = l_{i+1}}, \qquad i < m, \tag{18}$$

$$\chi_{i+1} = \frac{\phi_i \Lambda_{i+1}}{1 - \Delta_{i+1}}, \qquad i < m, \tag{19}$$

$$S_w \frac{\partial h_w}{\partial t} = G_{n_1}(b_1) r_w^{N_1 - 1 - \theta_1} K_1 \left(\frac{\partial h_1}{\partial r_1} \right)_{r_1 = r_w} + Q. \tag{20}$$

The transformation of equations (1), (9), (10), and (12) to equations (16)–(20) eliminates the radial scaling of storage and exchange area, while changing the diffusion dimensionality, and cancels the infinite-porosity inconsistency at the centre of the blocks (see section 3.4.1). Equation (16) is the standard diffusion equation in a space of dimension N_i with uniform specific storage S_{si}. However, the hydraulic conductivity is scaled by $K_i r_i^{-\theta_i}$, so the diffusivity $K_i r_i^{-\theta_i}/S_{si}$ is scaled accordingly. In the case of anomalous diffusion, the hydraulic conductivity tends to infinity at the centre of the blocks, but the no-flow boundary condition (8) maintains a finite flux. The exchange area density (19) can be rewritten as follows by using $\Lambda_{i+1} = \Delta_{i+1} n_{i+1}/l_{i+1}$:

$$\chi_{i+1} = \tau_i \Lambda_{i+1} = (\tau_i - \phi_i) n_{i+1}/l_{i+1}, \qquad i < m, \tag{21}$$

where τ_i is the effective fracture volume ratio, i.e., the ratio of porosity subject to diffusion to the fracture volume bounded by the complementary block distribution:

$$\tau_i = \phi_i/(1 - \Delta_{i+1}), \qquad i < m. \tag{22}$$

A value of $\tau_i = 1$ corresponds to a fully accessible fracture volume, while a value of $\phi_i < \tau_i < 1$ is used to model the existence of a nonaccessible fraction of the fracture volume (e.g., precipitation features or fracture filling).

2.6. Analytical Solutions

[21] In the Laplace domain, we obtain the following solutions for $\tilde{h}_w$, the drawdown in the well, and $\tilde{h}_1$, the drawdown at any location in domain P_1:

$$\tilde{h}_w = \frac{Q}{p} \frac{\mathrm{K}_{\nu_1}(\gamma_1 l_1^{E_1}) + \sigma_w \gamma_1 E_1 l_1^{E_1} \mathrm{K}_{\nu_1 - 1}(\gamma_1 l_1^{E_1})}{p S_w \mathrm{K}_{\nu_1}(\gamma_1 l_1^{E_1}) + \gamma_1 E_1 \left(G_{n_1}(b_1) K_1 l_1^{N_1 - E_1} + p S_w \sigma_w l_1^{E_1} \right) \mathrm{K}_{\nu_1 - 1}(\gamma_1 l_1^{E_1})} \tag{23}$$

and

$$\tilde{h}_1 = \frac{Q}{p} \frac{r_1^{\nu_1 E_1} \mathrm{K}_{\nu_1}(\gamma_1 r_1^{E_1})}{p S_w l_1^{\nu_1 E_1} \mathrm{K}_{\nu_1}(\gamma_1 l_1^{E_1}) + \gamma_1 E_1 \left(G_{n_1}(b_1) K_1 l_1^{N_1/2} + p S_w \sigma_w l_1^{\nu_1 E_1 + E_1} \right) \mathrm{K}_{\nu_1 - 1}(\gamma_1 l_1^{E_1})}, \tag{24}$$

where p is the Laplace variable and K is the modified Bessel function of the second kind. In equations (23) and (24) and later in equation (31) auxiliary variables are defined by:

$$E_i = (2 + \theta_i)/2 = \theta_i'/2, \tag{25}$$

$$\nu_i = 1 - N_i/2E_i = 1 - N_i'/2 \tag{26}$$

$$\gamma_m = \sqrt{p/\xi_m}/E_m, \tag{27}$$

$$\gamma_i = \sqrt{\frac{p}{\xi_i} + \frac{\lambda_{i+1} \gamma_{i+1} E_{i+1} l_{i+1}^{E_{i+1} - 1} \mathrm{I}_{1 - \nu_{i+1}}(\gamma_{i+1} l_{i+1}^{E_{i+1}})}{\mathrm{I}_{-\nu_{i+1}}(\gamma_{i+1} l_{i+1}^{E_{i+1}}) + \sigma_{i+1} \gamma_{i+1} E_{i+1} l_{i+1}^{E_{i+1}} \mathrm{I}_{1 - \nu_{i+1}}(\gamma_{i+1} l_{i+1}^{E_{i+1}})}} \Bigg/ E_i, \quad i < m, \tag{28}$$

where I is the modified Bessel function of the first kind, ξ_i is the diffusivity on the unit-radius hypersphere:

$$\xi_i = K_i/S_{si}, \tag{29}$$

and λ_{i+1} is the exchange coefficient:

$$\lambda_{i+1} = \chi_{i+1} l_{i+1}^{N_{i+1} - n_{i+1} - \theta_{i+1}} K_{i+1}/K_i, \qquad i < m. \tag{30}$$

The solutions $\tilde{h}_i$ for the drawdown at any location in domains P_i ($2 \leq i \leq m$) are obtained recursively for $\theta_i \geq -2$ and $N_i \geq n_i - 1$:

$$\tilde{h}_i = \tilde{h}_{i-1} \frac{r_i^{\nu_i E_i} \mathrm{I}_{-\nu_i}\left(\gamma_i r_i^{E_i}\right)}{l_i^{\nu_i E_i}\left(\mathrm{I}_{-\nu_i}\left(\gamma_i l_i^{E_i}\right) + \sigma_i \gamma_i E_i l_i^{E_i} \mathrm{I}_{1-\nu_i}\left(\gamma_i l_i^{E_i}\right)\right)}, \qquad (31)$$

where the auxiliary variables are defined by equations (25)–(28). Time-resolved drawdowns h_w and h_i, $1 \leq i \leq m$, can be obtained using the algorithm by *Stehfest* [1970]. Appendix A presents a full derivation of the solutions presented above, while Appendix B gives an analysis of the consistency of these solutions with numerical considerations. Note that, although θ_i is usually considered positive in hydrology applications, the above solutions are valid for negative values of θ_i (i.e., superdiffusion).

3 Discussion

3.1 Examples of Application

[22] Appropriately, this model is applicable when the pumping chamber intercepts the most conductive fracture network. Indeed, the hydrodynamic consistency of the model implies that $K_{i<m} \gg K_{i+1}$, because we assume by construction that exchanges between the pumping well and domains $P_{i>1}$ are minor compared to exchanges with P_1. Similarly, we assume that exchanges between domain P_i and the domains $P_{j>i+1}$ are minor compared to exchange with P_{i+1}.

[23] This approach gives rise to two important remarks. Firstly, fracture network is used here as a generic term for any type of structured network of planar drains delimiting permeable regions where hydrodynamic properties are distinctly different. This model can handle specific network geometries and properties for each conductive level. Note that linear drains cannot be modeled because they do not subdivide the embedding rock into segregated blocks, and thus they do not drain them peripherally. Secondly, in this model, the fractal behavior of the flow in a given domain reflects the fractal diffusion properties in a similar way to the approach proposed by *Acuna and Yortsos* [1995]. However, our model differentiates the properties for each conductive domain level, so it is suitable for simulating a hierarchy of discontinuities that can have distinctly different origins and ages leading to contrasted properties. In the following, we give some examples of field applications.

[24] 1. In stratified aquifers, permeability discontinuities are common at the layer interfaces. Each layer may correspond to a fractured medium. The fracture network in the layers have clearly different origins and flow properties from the horizontal permeable discontinuity at the layer interface. When intersected by a pumping well, the (fractal) density dimension of the subparallel horizontal planar drains is $N_1 \leq 2$. These planar drains delimit blocks with $N_2 = 1$. Blocks delimited by the fracture network embedded in the layers are drained peripherally, so that $N_3 \leq 3$. Fractal flow in the layer discontinuities will result, for example, from the distribution of connected zones with non-null aperture, whereas the fractal flow in blocks will result from fracture properties including length, aperture, orientation and density.

[25] 2. If a pumping well crosses a (sub)vertical fault ($N_1 = 1$), the fault may delimit two large-fractured blocks ($N_2 = 1$), whose half-thickness is the mean distance to an impervious boundary. The fracture network of porosity domain P_2 peripherally drains the matrix blocks ($N_3 \leq 3$). The vertical fault can result from present-day shear forces, while P_2 fracture networks can result, for example, from a previous episode of large-scale distension.

[26] 3. Karstified fracture networks are formed by dissolution of preexisting discontinuities. In many cases, the entire aquifer is later subject to extensional stresses that create a secondary fracture network delimiting permeable matrix blocks. Pumping tests in such hierarchized systems show that karstified fracture networks usually dominate flow at the large scale ($N_1 \leq 3$), while local flow is controlled by small fractures ($N_2 \leq 3$) delimiting matrix blocks ($N_3 \leq 3$).

3.2. Fracture Aperture Determination

[27] The fracture aperture e_i is obtained from equation (22):

$$e_i = l_{i+1}\left[\left(\frac{\alpha_{n_{i+1}}}{n_{i+1}(1-\phi_i/\tau_i)}\right)^{1/n_{i+1}} - 2\beta_{i+1}\right], \qquad i < m. \qquad (32)$$

Note that e_i is the geometrical aperture, but this does not correspond in general to the hydraulic aperture. The fracture aperture e_i depends on the complementation model (either block volume or exchange area equivalence) used to transform hypercubic blocks to hyperspheric blocks (equation (32) and Table 2). Figures 6 shows the relation between the dimensionless groups e_i/l_{i+1}, ϕ_i/τ_i and n_{i+1}, for equivalence of volume and exchange area between hyperspheric and hypercubic blocks. In fractured media, the region of interest for the parameters is typically defined by $e_i/l_{i+1} < 10^{-1}$, $\phi_i < 10^{-1}$ and $\tau_i = 1$. Consequently, the volume equivalence model is the most relevant for modeling fractured media, because $e_i/l_{i+1} > 10^{-1}$ for the exchange area equivalence model. Furthermore, the exchange area equivalence model presents an important defect: the shape factor β is not defined for $n = 1$ because the exchange area does not depend on the block thickness, and therefore any value of the shape factor satisfies the exchange area equivalence. In the following simulations we will use the volume equivalence model.

3.3. Parameter Equivalence With Other Published Models

[28] The present study generalizes all the previous published models accounting for fractal properties and anomalous diffusion (Table 1). Compared with the single-porosity fractal model by *Chang and Yortsos* [1990], i.e., equation (16) with $q_1 = 0$, our model adds a theoretically unbounded number of nested fractal porosity levels. The more restricted model by *Barker* [1988] is reproduced by setting a fractional dimension shape for the well exchange chamber, while considering $\theta_1 = 0$ and $n_1 = N_1$ which is the fractional flow dimension.

[29] Compared with the double-porosity fractional flow model by *Hamm and Bidaux* [1996], our model takes into account the anomalous diffusion in the first porosity domain, adding generalized block shape along with fractal diffusion in the blocks and further fractal porosity levels. The model by *Hamm and Bidaux* [1996] is reproduced by setting $q_1 \neq 0$, $q_2 = 0$, $n_2 = N_2 = 1$ and $\theta_2 = 0$. The exchange coefficient implemented in their model (i.e., $\chi_2 = 1/l_2$) is

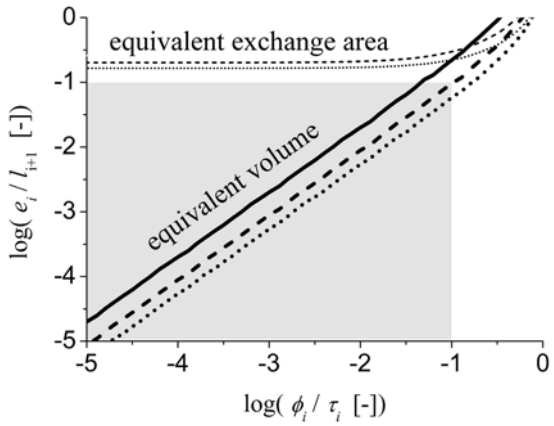

Figure 6. Relation between the parameters e_i/l_{i+1} and ϕ_i/τ_i assuming exchange area equivalence and volume equivalence between hyperspherical and hypercubic blocks. For better visibility, only the curves for integral values of the block shape dimension are represented: $n_{i+1} = 1$ (solid), $n_{i+1} = 2$ (dashed), $n_{i+1} = 3$ (dot). The region denoting the commonly used values for the parameters in fractured media is shaded.

obtained by setting in equation (21) $e_1 \ll l_2$ in Λ_2 or $\phi_1 \ll \tau_1$, and $\tau_1 = 1$.

[30] The triple-porosity model proposed by *Rodriguez et al.* [2004] does not account for fractal properties. Their approach is reproduced in our model by assuming $q_1 \neq 0$, $q_2 \neq 0$, $q_3 = 0$, $N_1 = n_1 = 2$, $\theta_1 = 0$, and high fracture skin factors σ_2 and σ_3. Since the type of exchange modeled by *Rodriguez et al.* is stationary, it does not take of account for flow dimensions N_2 and N_3, anomalous diffusion exponents θ_2 and θ_3, or block shape dimensions n_2 and n_3.

3.4. Model Consistency

3.4.1. Porosity Scaling

[31] By construction, the scaling law (equation (4)) leads to an inconsistency in the definition of porosity ϕ_{fi}, which tends to infinity if $N_i < n_i$ when r_i tends to 0. This occurs at the centre of the blocks or at the source in the case of an infinitesimal source. Note that a lower scale cutoff would prevent this effect, but so far there are no analytical solutions accounting for scale cutoffs. This inconsistency disappears when projecting the diffusion equations (1), (9), (10), and (12) into the space of dimension N_i (equations (16)–(20)), while applying a rigorous match of the flow equipotential and the exchange area at the exchange interfaces. This matching is applied between the source and the domain P_1, as well as between each domain pair P_i, P_{i+1}. An exact match is obtained by accepting fractional values to characterize the dimension of the well exchange chamber and the block, and fixing $n_i = N_i$, similarly to the approach proposed in the models by *Barker* [1988] and *Hamm and Bidaux* [1996]. This cancels the porosity scaling and provides the advantage of eliminating the fitting parameters n_i, which are not known a priori.

3.4.2. Parameter Simplification in Domain P_1

[32] Pumping chamber shape parameters n_1 and b_1 can always be reduced conveniently and without loss of generality. This is because, for any model characterized by distinct values of n_1 and N_1, there is an equivalent model with $n_1 = N_1$ but with a different value of b_1. Since n_1 and b_1 are used to parameterize the well (for aquifer exchange only, i.e., equation (20)), both models are equivalent if they define the same exchange rate. This condition is satisfied when

$$\mathrm{G}_{n_1}(b_1) = \mathrm{G}_{N_1}\left(\bar{b}_1\right), \tag{33}$$

where $\bar{b}_1$ is the orthoradial length of the pumping chamber for $n_1 = N_1$. For nonintegral dimensions, the physical meaning of the orthoradial length is obscure. A practical way to apply equation (33) is to set $\bar{b}_1 = 1$ and $n_1 = N_1$. In this way, we eliminate parameters n_1 and b_1 while ensuring a rigorous match of the equipotentials at the pumping chamber periphery.

3.4.3. Miscellaneous Remark

[33] Although commonly used, the assumption of uniform pressure stress at the periphery of the blocks is clearly not valid for large block radius when pressure gradients are high. This situation may occur particularly close to the source for P_2 blocks or close to the periphery of the P_i blocks in the case of P_{i+1} blocks with $m > i \geq 2$.

3.5. Sensitivity Analysis and Parameter Reduction

[34] In the next sections, we use synthetic examples to illustrate the effects of fractal dimension, anomalous diffusion, flow dimension, multiporosity and well storage.

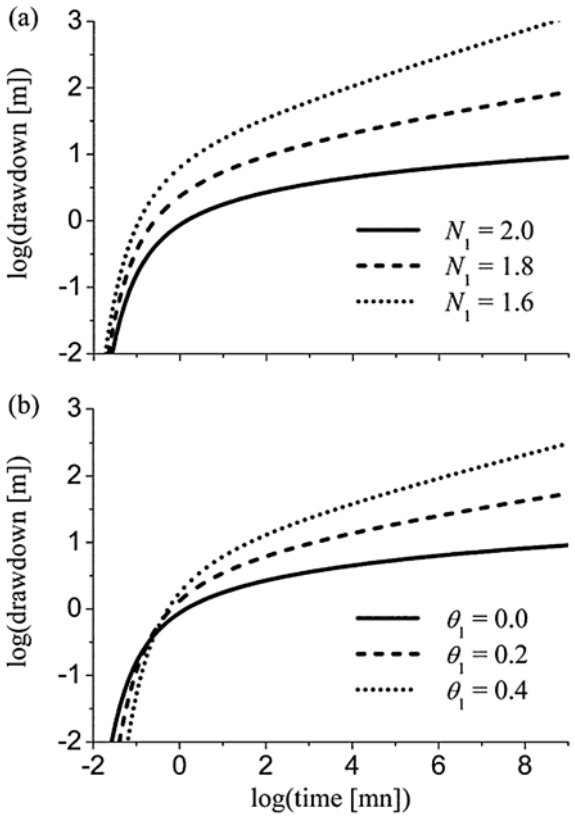

Figure 7. Example of time-resolved head responses in a piezometer ($r_1 = 40$ m) assuming a single-porosity system. Results show the effect of changing N_1 and θ_1. Simulations are performed using an infinitesimal source solution with $K_1 = 10^{-4}$ m s^{-1}, $S_{s1} = 10^{-6}$ m^{-1}, $Q = 5 \times 10^{-4}$ m^3 s^{-1}, and by default $N_1 = 2$ and $\theta_1 = 0$.

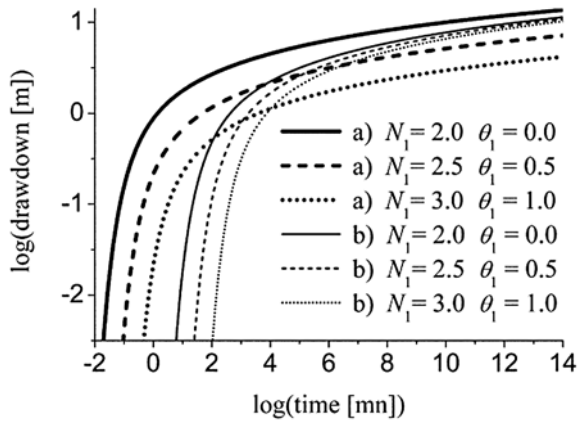

Figure 8. Example of time-resolved head responses in a piezometer, assuming a single-porosity system. Results show the effect of changing θ_1 while the flow dimension is kept constant ($N'_1 = 2$). Simulations are performed using an infinitesimal source solution with $Q = 5 \times 10^{-4}$ m^3 s^{-1}. (a) Thick curves are computed for $r_1 = 40$ m with $K_1 = 10^{-4}$ m s^{-1}, $S_{s1} = 10^{-6}$ m^{-1}. (b) Thin curves are computed for $r_1 = 700$ m with the parameters presented in Table 3.

[35] In the following examples, fracture apertures are determined by equation (32), with $\tau_i = 1$ by default, and we apply the shape factor (Table 2) such that hyperspherical and hypercubic blocks have the same volume rather than the same exchange area (see section 3.2). Moreover, we apply an exact match of the flow equipotential and exchange area at the exchange interfaces ($n_i = N_i$), while setting the orthoradial length of the pumping chamber as $\bar{b}_1 = 1$.

3.5.1. Single Porosity

[36] Results for single porosity are given in Figures 7 and 8 for different values of N_1 and θ_1 using the infinitesimal source solution (equation (C6)). This solution assumes that well storage is nil ($S_w = 0$) and source size is negligible compared to the distance from the well. In these examples, skin effects are not considered.

[37] Figure 7 shows the different effects on the drawdown produced by changing N_1 and θ_1. By decreasing N_1 and increasing θ_1, we obtain a similar increase in the late-stage drawdown. This is because both changes lead to a decrease in the flow dimension (equation (5)). These effects can be best discriminated on the basis of the early response. Decreasing N_1 causes an early response because it acts by decreasing the fractal volume and therefore leads to a prompt response, whereas increasing θ_1 delays the response because it acts by decreasing the diffusion.

[38] In Figure 8, the curves labeled a refer to a piezometer positioned 40 m from the source, while curves labeled b are computed assuming a distance of 700 m. Curves a show the effects of changing θ_1 on the drawdown at constant flow dimension N'_1, according to equation (5). We observe that the response time increases with θ_1 (because diffusion decreases). As demonstrated in Appendix C, we can reproduce the curve a computed with $\theta_1 = 0$, $K_1 = 10^{-4}$ m s^{-1} and $S_{s1} = 10^{-6}$ m^{-1}, by increasing θ_1 (e.g., $\theta_1 = 0.5$ or 1), while keeping the same flow dimension, and also decreasing K_1 and S_{s1}, using equations (C7) and (C8), respectively. Thus we obtain three simulations with the same flow dimension and distinct values of θ_1, K_1, S_{s1} and N_1 (see Table 3). These three models display identical transient drawdown at $r_1 = 40$ m, but different drawdown at $r_1 = 700$ m (curves b in Figure 9). This emphasizes that, to determine θ_1, we require at least two piezometers situated at distinctly different distances from the pumping well (Table 4).

3.5.2. Double Porosity

[39] The double-porosity behavior can be investigated using the curves presented in Figure 9a. This figure shows the drawdown computed for a piezometer at a given small distance from the pumping well.

[40] For a piezometer intercepting the first porosity (curve 2PorPz1 in Figure 9), mainly the first porosity network is drained at the beginning of the test, and the double-porosity response is identical to that exhibited by a single porosity (curve 1Por (S1)) with conductivity K_1 and specific storativity S_{s1}. Then, the second porosity is progressively drained and the response becomes that of a single

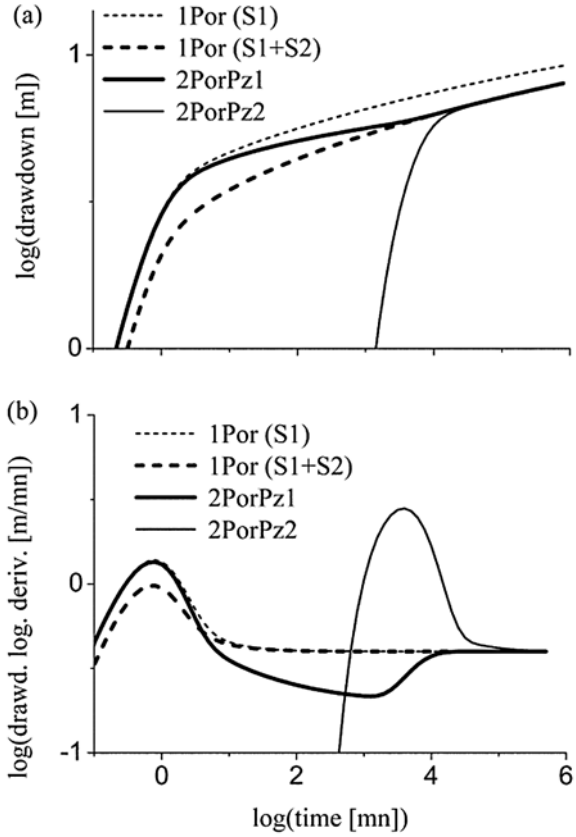

Figure 9. Example of time-resolved head responses in a piezometer assuming a double-porosity system. Results show the effects of double porosity and well storage. Simulations are performed with the parameters presented in Table 4 with normal transport, no skin effect, $S_w = 2.82 \times 10^{-4}$ m^2, $r_w = 5 \times 10^{-2}$ m, and $Q = 5 \times 10^{-4}$ m^3 s^{-1} (for $\phi_i = 10^{-3}$, $e_1 = 2 \times 10^{-3}$ m). Drawdowns (a) and logarithmic derivatives of drawdown (b) are presented for a piezometer intercepting the first porosity alone (curve 1Por(S1)), the first porosity draining the second porosity (curve 2PorPz1), the first porosity alone with storage equal to $S_{s1} + S_{s2}$ (curve 1Por(S1 + S2)) and for a piezometer in the second porosity (curve 2PorPz2).

Table 3. Parameters Used in Figure 8 Producing the Same Transient Drawdown at $r_1 = 40$ m

N_1 (−)	θ_1 (−)	K_1 (m/s)	S_{s1} (m^{-1})
2.0	0.0	10^{-4}	10^{-6}
2.5	0.5	5.446×10^{-5}	1.345×10^{-7}
3.0	1.0	3.333×10^{-5}	1.875×10^{-8}

porosity model (curve 1Por(S1 + S2)) with conductivity K_1 and specific storage $S_{s1} + S_{s2}$. For a piezometer in the second porosity (curve 2PorPz2), the response is delayed and the late-time behavior is that of the model producing curve 1Por(S1 + S2).

[41] The logarithmic derivative of drawdown ($\partial h/\partial \ln(t)$) is more sensitive than its primitive, thus providing another fitting curve that is helpful for discriminating the model type [*Bourdet et al.*, 1983]. Figure 9b shows a plot of the logarithmic derivatives. Wellbore storage produces an initial linear increase, which, in the course of time, is followed by a decrease of the drawdown derivative. For a piezometer intercepting the first porosity, the double-porosity effect is expressed as a U-shaped perturbation corresponding to the progressive drainage of the second porosity. It can be superimposed onto the wellbore storage effect.

[42] Figure 10 presents curves illustrating the effects of the parameters on the transition period without wellbore storage. This figure shows the drawdown logarithmic derivative for a piezometer intercepting the first porosity at a given small distance from the pumping well.

[43] We observe that the U-shaped curves are related to high values of S_{s2} (Figures 10a, 10b, and 10e) and high values of τ_1 (Figure 10h). The end of the transition is delayed when S_{s2} increases because of the smaller block diffusivity. The time at which the transition starts decreases when S_{s2} increases. Indeed, higher values of S_{s2} induce higher exchanges caused by the smaller diffusivity in the blocks, which leads to higher head gradient at the interface. Similarly, higher values of τ_1 induce higher exchanges caused by the higher exchange area density. The effect of changing the exchange area density χ_2 can be parameterized by τ_1 because τ_1 only appears in χ_2 (equation (21)). Higher values of χ_2 (higher τ_1 in Figure 10h) brings forward the start of the transition while not affecting the end of the transition.

[44] The V-shaped curves are related to high skin factors (Figure 10i), and a high anomalous diffusion exponent (Figure 10f). The V shape is typical of the stationary exchange model, which assumes instantaneous diffusion in the blocks. For high values of σ_2, the exchange is controlled by the reduction in permeability at the interface, rather than by the diffusive properties of the block. On the other hand, the diffusion increases with θ_2 because diffusivity increases from the block periphery to the centre. Note the important advantage of using transient rather stationary exchange model, since the latter allows V-shaped curves only.

[45] A shift in time is produced by changing parameters N_2, σ_2, K_2 and l_2. The parameters N_2 and σ_2 influence the amplitude of the transition perturbation, with higher N_2 smoothing the transition (Figure 10c) and higher σ_2 producing a sharper transition (Figure 10i). K_2 and l_2 are the only parameters that do not influence the amplitude of the transition perturbation, since they produce a simple horizontal translocation (Figures 10d and 10g). Their effect on the transition is the same. Indeed, in the first porosity drawdown (equation (24)), K_2 and l_2 only have an influence on γ_1 (equation (28) with $i = 1$) via the terms $\lambda_2\gamma_2 l_2^{E_2-1}$ and $\gamma_2 l_2^{E_2}$. In these terms, K_2 and l_2 can be combined together into $\sqrt{K_2}/l_2^{1+\theta_2/2}$, such that, for any value $\bar{K}_2$ we can find a value $\bar{l}_2$ that keeps the first porosity drawdown unchanged:

$$\bar{l}_2 = l_2(\bar{K}_2/K_2)^{1/(2+\theta_2)} \tag{34}$$

The curves (Figure 10g) are generated from Figure 10d using equation (34). However, this procedure affects the drawdown in the second porosity. Thus to carry out fitting when no data is available in the second porosity, one of these parameters can be assigned a fixed value. Otherwise, if data is available in the second porosity, the first porosity drawdown can be fitted first with one parameter fixed, and then the second porosity drawdown can be fitted by relaxing that parameter and adapting the other with equation (34).

[46] The onset of the transition is affected by all the parameters but θ_2 (Figure 10f). In detail, the onset of the transition is delayed (1) by setting a smaller value of S_{s2} or τ_1 as stated above, (2) by setting a smaller value of K_2 or a higher value of σ_2 which both decrease the exchange rate, and (3) by setting a smaller value of N_2 or a higher value of l_2, which act as decreasing the exchange area density (21).

[47] The end of the transition is affected by all the parameters, except if K_2 or S_{s2} are modified while keeping ξ_2 constant (Figure 10e) and by modifying τ_1 (Figure 10h). These two modifications produce the same effect, since they both ensure that the diffusivity equation (16, $i = 2$) remains unchanged. Hence for any value of K_2, it is possible to keep λ_2 constant by assigning:

$$\tau_1 = \phi_1 + \frac{\lambda_2 K_1 l_2^{\theta_2+1}}{K_2 n_2} \tag{35}$$

The curves in Figure 10h are generated from Figure 10e using equation (35). Thus for fitting, one of these parameters can be fixed by assigning a value. However, the value of τ_1 is limited by two bounds and can lead to unrealistic fracture apertures. Since K_2 is limited by only one bound, it is more convenient to fix τ_1 and vary K_2. Note that, because ξ_2 and λ_2 are kept constant, the end of the transition is unaffected by S_{s2} when $S_{s1} + S_{s2}$ remains constant for $S_{s1} \ll S_{s2}$ (Figure 10b).

[48] The above considerations lead to the following steps to iterate for the inversion of parameters: (1) fit the end of the transition using K_2, (2) fit the start of the transition using S_{s2} with constant ξ_2, (3) fit the shape of the transition perturbation using N_2, θ_2, and σ_2, and (4) fit the second porosity drawdown using l_2 and K_2 (equation (34)).

Table 4. Parameters of P_i Domains Used for Figures 9 and 10

i	K_i (m/s)	S_{si} (m^{-1})	N_i (−)	l_i (m)	r_i (m)
1	10^{-4}	10^{-6}	2	0.05	1
2	4×10^{-11}	1.9×10^{-5}	1	1	0

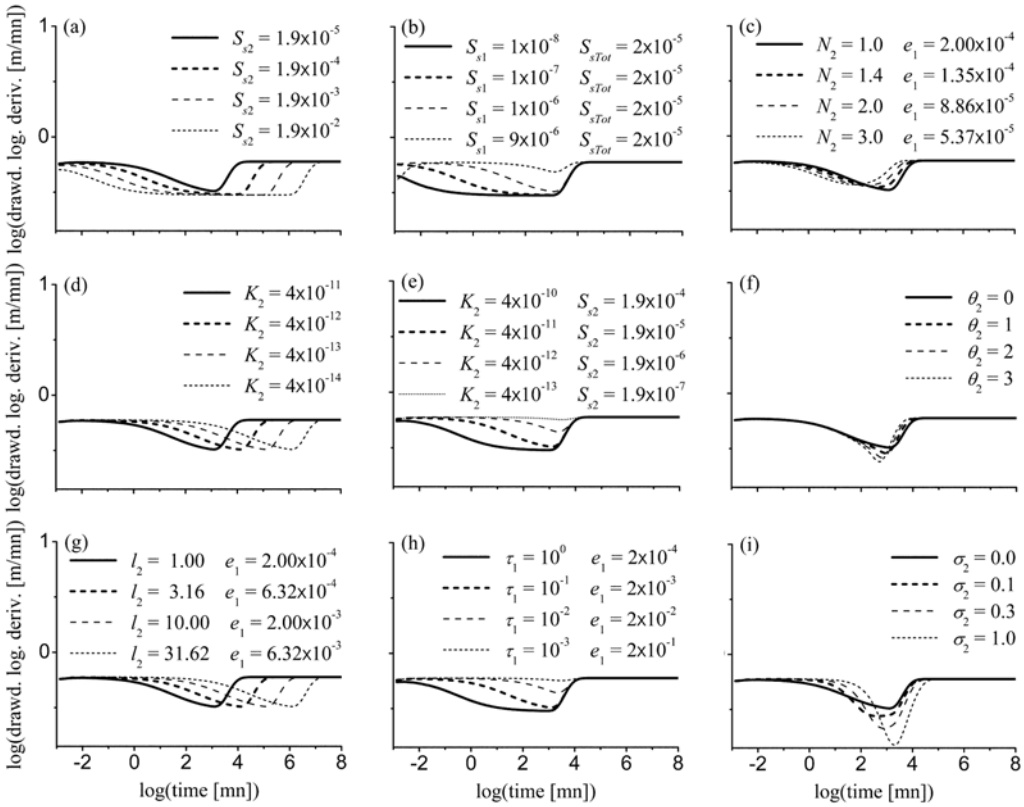

Figure 10. Example of time-resolved response of logarithmic derivatives of head in a piezometer intercepting the first porosity of a double-porosity system. Results show the effect of parameters on the transition period, without well storage. Simulations are performed using the parameters presented in Table 4, with normal transport and no skin effect, $r_w = 5 \times 10^{-2}$ m and $Q = 7.5 \times 10^{-4}$ m^3 s^{-1} (for $\phi_1 = 10^{-3}$, $e_1 = 2 \times 10^{-3}$ m). The curves are computed by modifying only the parameters specified in the legend: (a) S_{s2}, (b) S_{s2} with constant $S_{s\text{Tot}} = S_{s1} + S_{s2}$, (c) N_2, (d) K_2, (e) K_2 and S_{s2} with constant $\xi_2 = K_2/S_{s2}$, (f) θ_2, (g) l_2, (h) τ_1, (i) σ_2.

3.5.3. *m* Porosities (*m* > 2)

[49] Figure 11a shows the responses of a piezometer in the first domain of a triple-porosity system at a given distance from a pumping well in a sedimentary aquifer. In these simulations, the well taps layer discontinuities (P_1) delimiting planar blocks (P_2), while these blocks are themselves subdivided by vertical fractures that segregate porous matrix sub-blocks (P_3). The parameters given in Table 5 represent standard values for karstic aquifer. In contrast to the double-porosity effect (Figure 9), the response displayed by curve 3PorPz1(1) shows that the drainage of the third porosity can produce a second drawdown inflexion and a second transition of the drawdown logarithmic derivative (Figure 11b). In a final stage, the behavior becomes identical to that exhibited by a single porosity system (curve 1Por(S1 + S2 + S3)), with conductivity K_1 and specific storage $S_{s1} + S_{s2} + S_{s3}$. The triple-porosity parameters have effects on the second transition period that are analogous with those illustrated above for the transition period of the double-porosity model (Figure 10). The response displayed by curve 3PorPz1(2) shows that it can be difficult to investigate the triple-porosity effect using the drawdown logarithmic derivative when there is a weak conductivity contrast between domains.

[50] More generally, for system with m domains, the response of a piezometer in the first domain can show $m - 1$ transitions of the drawdown logarithmic derivative before reaching a terminal behavior identical to that observed for a single porosity with conductivity K_1 and specific storage $S_{s1} + S_{s2} + \ldots + S_{sm}$.

4. Conclusion and Remarks

[51] In the present model, we assume a nested distribution of fractured networks. Nested fracture models are a specific case of multicontinuum models in which porosity domains are hierarchically drained so the number of domain-to-domain flow exchange interfaces is equal to the number of domain minus one. In the case of pumping tests, the higher permeability domain will exchange flow with the pumping well. Each fractured network is characterized by its porosity and permeability, and may not only display fractal geometry but also produce anomalous diffusion. Compared to others published models, the approach presented here combines multifractal diffusion and multiporosity with transient exchanges, interface skin effects and well storage effects.

[52] The proposed analytical solution in the Laplace domain allows us to calculate drawdown at the pumping well and at any distance from the well for each porosity level. After numerical inversion, the solution in the time-space domain yields a large spectrum of time-resolved

drawdown curves, including those obtained using the models by *Barker* [1988], *Chang and Yortsos* [1990], and *Hamm and Bidaux* [1996]. While hydrology applications usually assume subdiffusion, with porosity, hydraulic conductivity, specific storativity and diffusivity decreasing as a function of increasing radial distance, our model allows the study of superdiffusion in all the domains, with diffusivity increasing as a function of increasing radial distance.

[53] To ensure geometrical consistency and reduce the number of fitting parameters, we introduce two conceptual approaches:

[54] 1. By applying the fractional dimension shape, we generalize block and pumping well shapes to nonintegral dimensions, allowing an exact match between block periphery and within block equipotential, and also between the pumping chamber periphery and external equipotentials. At the same time, we can eliminate the orthoradial length of the pumping chamber, which is an obscure parameter for nonintegral dimensions.

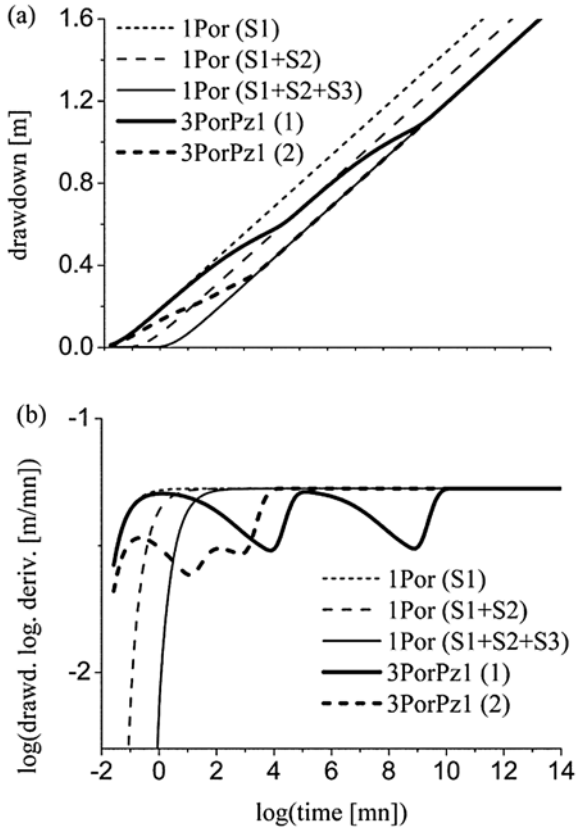

Figure 11. Example of time-resolved head responses in a piezometer (r_1 = 200 m) intercepting the first porosity of a triple-porosity system. Results show the triple-porosity effect. Simulations are performed with the parameters presented in Table 5 with normal transport, no skin effect, no well effect, $\tau_1 = 1$, $r_w = 5 \times 10^{-2}$ m, and $Q = 6.67 \times 10^{-3}$ m^3 s^{-1}. For a porosity value of 10^{-4}, the fracture aperture values of the first and second porosities are 10^{-2} and 10^{-3} m, respectively. Drawdowns (a) and logarithmic derivatives of drawdown (b) are computed for a piezometer intercepting the first porosity alone (curve 1Por(S1)), the first porosity alone with storage equal to $S_{s1} + S_{s2}$ (curve 1Por(S1 + S2)), the first porosity alone with storage equal to $S_{s1} + S_{s2} + S_{s3}$ (curve 1Por(S1 + S2 + S3)) and the first porosity draining the second and third porosities, using the conductivities in Table 5(1) (curve 3PorPz1(1)), and the conductivities in Table 5(2) (curve 3PorPz1(2)).

Table 5. Parameters of P_i Domains Used for Figure 11

i	(1) K_i (m/s)	(2) K_i (m/s)	S_{si} (m^{-1})	N_i (−)	l_i (m)
1	10^{-2}	10^{-2}	10^{-6}	2	0
2	10^{-8}	10^{-5}	10^{-5}	1	50
3	10^{-14}	10^{-8}	10^{-4}	1	5

[55] 2. Rules are defined for fracture-block complementation in order to ensure consistency between porosity, fracture aperture and block shape, while also eliminating one of the fitting parameters (usually the fracture aperture). Equations are derived for both volume and exchange area equivalence between hypercubic blocks and hyperspherical blocks. Yet we show that the volume equivalence model is more pertinent to model fractured aquifers than the exchange area equivalence model. We point out that volume complementation was not addressed in previous modeling studies. Provided volume complementation is performed, we can rigorously define the geometrical parameter τ_i accounting for the occurrence of nonconductive zones (e.g., due to precipitation features or clogging).

[56] While this model allows the simulation of a wide range of situations, there are some remaining limitations. The main one is certainly the obligatory hierarchy of the properties; conductivity of each fracture network must be distinctly different from the others networks, but it is worth noticing that fracture sets with weakly different conductivities can be modeled by a single continuum with averaged properties. Another limitation discussed in section 3.1 is the impossibility to model linear drains because they do not subdivide the embedding rock into segregated blocks, and thus they do not drain them peripherally. Also, as usual in the analytical models (i.e., listed in Table 1) fractal scale cutoffs are not accounted for. In our model, the upper scale cutoff in the blocks is implicitly greater than the block radius, but fractal properties are assumed to have no lower scale cutoff.

Appendix A: Solutions in the Laplace Domain

[57] By applying a Laplace transform with respect to time and using the initial conditions (equations (6) and (15)), we obtain from equations (16)–(19) the following diffusion equations:

$$\frac{p}{\xi_i} r_i^{\theta_i} \tilde{h}_i = \frac{(N_i - 1 - \theta_i)}{r_i} \frac{d\tilde{h}_i}{dr_i} + \frac{d^2\tilde{h}_i}{dr_i^2} - \lambda_{i+1} r_i^{\theta_i} \left(\frac{d\tilde{h}_{i+1}}{dr_{i+1}} \right)_{r_{i+1}=1_{i+1}}, \quad i < m, \tag{A1}$$

$$\frac{p}{\xi_m} r_m^{\theta_m} \tilde{h}_m = \frac{(N_m - 1 - \theta_m)}{r_m} \frac{d\tilde{h}_m}{dr_m} + \frac{d^2\tilde{h}_m}{dr_m^2}, \tag{A2}$$

the boundary conditions (7) and (8) are:

$$\lim_{r_1 \to +\infty} \tilde{h}_1 = 0 \tag{A3}$$

$$\lim_{r_1 \to 0} \left(r_i^{N_i - n_i - \theta_i} \frac{\partial \tilde{h}_i}{\partial r_i} \right) = 0, \qquad i > 1, \tag{A4}$$

the fracture skin equation (11) is:

$$\tilde{h}_{i-1} = \left(\tilde{h}_i + l_i \sigma_i d\tilde{h}_i / dr_i \right)_{r_i = l_i}, \qquad i > 1, \tag{A5}$$

the pumping chamber mass balance differential equation (20) is:

$$S_w p \tilde{h}_w = \mathrm{G}_{n_1}(b_1) r_w^{N_1 - 1 - \theta_1} K_1 \left(\frac{d\tilde{h}_1}{dr_1} \right)_{r_1 = r_w} + \frac{Q}{p}, \tag{A6}$$

and the pumping chamber skin equation (13) is:

$$\tilde{h}_w = \left(\tilde{h}_1 - r_w \sigma_w d\tilde{h}_1 / dr_1 \right)_{r_1 = r_w}. \tag{A7}$$

[58] For domain P_m, the general solution of equation (A2) is:

$$\tilde{h}_m = C_{1m} r_m^{\nu_m E_m} \mathrm{I}_{\nu_m}\left(\gamma_m r_m^{E_m}\right) + C_{2m} r_m^{\nu_m E_m} \mathrm{K}_{\nu_m}\left(\gamma_m r_m^{E_m}\right), \tag{A8}$$

where I and K are the modified Bessel functions of the first and second kind, respectively, with C_{1i} and C_{2i}, $i = 1, \ldots, m$, are integration variables, while assuming the following:

$$E_m = (2 + \theta_m)/2, \tag{A9}$$

$$\nu_m = 1 - N_m/(2E_m), \tag{A10}$$

$$\gamma_m = \sqrt{p/\xi_m}/E_m. \tag{A11}$$

The auxiliary variables ν_m and γ_m must be finite. This implies that E_m must be nonzero and therefore $\theta_m \neq -2$. Because θ_m should range in an interval containing 0, we assume $\theta_m > -2$ in the following. For x, y, Z real, we use:

$$(d/dZ)(Z^x \mathrm{I}_x(yZ)) = yZ^x \mathrm{I}_{x-1}(yZ), \tag{A12}$$

$$(d/dZ)(Z^x \mathrm{K}_x(yZ)) = -yZ^x \mathrm{K}_{x-1}(yZ), \tag{A13}$$

yielding:

$$d\tilde{h}_m/dr_m = \gamma_m E_m r_m^{\nu_m E_m + E_m - 1}\left(C_{1m}\mathrm{I}_{\nu_m - 1}\left(\gamma_m r_m^{E_m}\right) - C_{2m}\mathrm{K}_{\nu_m - 1}\left(\gamma_m r_m^{E_m}\right)\right). \tag{A14}$$

Since $\nu_m - 1 < 0$, and using the reflection formulae:

$$\mathrm{K}_x(Z) = \mathrm{K}_{-x}(Z), \qquad Z > 0, \tag{A15}$$

$$\mathrm{I}_x(Z) = \mathrm{I}_{-x}(Z) + 2\sin(-x\pi)\mathrm{K}_{-x}(Z)/\pi, \qquad Z \geq 0, \tag{A16}$$

we obtain, with $\sin(\nu_m \pi) = \sin((1 - \nu_m)\pi)$:

$$d\tilde{h}_m/dr_m = \gamma_m E_m r_m^{\nu_m E_m + E_m - 1}\left[C_{1m}\mathrm{I}_{1-\nu_m}\left(\gamma_m r_m^{E_m}\right) + (2C_{1m}\sin(\nu_m\pi)/\pi - C_{2m})\mathrm{K}_{1-\nu_m}\left(\gamma_m r_m^{E_m}\right)\right]. \tag{A17}$$

Using the asymptotic behaviors:

$$\mathrm{I}_x(Z) \approx (Z/2)^x/\Gamma(x+1), \qquad x \geq 0, \qquad 0 \leq Z \ll \sqrt{x+1}, \tag{A18}$$

$$\mathrm{K}_x(Z) \approx (Z/2)^{-x}\Gamma(x)/2, \qquad x > 0, \qquad 0 < Z \ll \sqrt{x+1}, \tag{A19}$$

we obtain for $0 < \gamma_m r_m^{E_m} \ll \sqrt{2 - \nu_m}$:

$$d\tilde{h}_m/dr_m \approx \eta_1 C_{1m} r_m^{2E_m - 1} + \eta_2 (2C_{1m}\sin(\nu_m\pi)/\pi - C_{2m}) r_m^{2\nu_m E_m - 1}, \tag{A20}$$

where:

$$\eta_1 = \frac{\gamma_m^{2-\nu_m} E_m}{2^{1-\nu_m}\Gamma(2-\nu_m)}, \tag{A21}$$

$$\eta_2 = \frac{\gamma_m^{\nu_m} E_m \Gamma(1-\nu_m)}{2^{\nu_m}}. \tag{A22}$$

In equation (A20), η_1 and η_2 are not always zero because $E_m > 0$, $1 - \nu_m > 0$, and $\gamma_m > 0$ for $p > 0$, so the boundary condition (A4), $(i = m)$ is satisfied for:

$$C_{2m} = 2C_{1m}\sin(\nu_m\pi)/\pi, \tag{A23}$$

because $N_m - n_m - \theta_m + 2\nu_m E_m - 1$ is negative or nil, and for:

$$N_m > n_m - 1, \tag{A24}$$

such that $N_m - n_m - \theta_m + 2E_m - 1 > 0$. Hence we obtain:

$$d\tilde{h}_m/dr_m = C_{1m}\gamma_m E_m r_m^{\nu_m E_m + E_m - 1}\mathrm{I}_{1-\nu_m}\left(\gamma_m r_m^{E_m}\right), \tag{A25}$$

and with equation (A16):

$$\tilde{h}_m = C_{1m} r_m^{\nu_m E_m}\mathrm{I}_{-\nu_m}\left(\gamma_m r_m^{E_m}\right). \tag{A26}$$

The fracture skin equation (A5, $i = m$) with equation (A25) gives:

$$C_{1m} = \tilde{h}_{m-1}/A_m, \tag{A27}$$

where:

$$A_m = l_m^{\nu_m E_m}\left[\mathrm{I}_{-\nu_m}\left(\gamma_m l_m^{E_m}\right) + l_m^{E_m}\sigma_m\gamma_m E_m \mathrm{I}_{1-\nu_m}\left(\gamma_m l_m^{E_m}\right)\right], \tag{A28}$$

which gives:

$$\tilde{h}_m = \tilde{h}_{m-1} r_m^{\nu_m E_m} \mathrm{I}_{-\nu_m}\left(\gamma_m r_m^{E_m}\right)/A_m. \quad \text{(A29)}$$

By substituting in the exchange term of domain P_{m-1}, combining equation (A25) with equation (A27) gives:

$$\left(d\tilde{h}_m/dr_m\right)_{r_m=l_m} = \tilde{h}_{m-1} B_m, \quad \text{(A30)}$$

where:

$$B_m = \bar{A}_m/A_m, \quad \text{(A31)}$$

$$\bar{A}_m = l_m^{\nu_m Em+Em-1} \gamma_m E_m \mathrm{I}_{1-\nu_m}\left(\gamma_m l_m^{E_m}\right). \quad \text{(A32)}$$

Using equation (A30), the diffusion equation (A1, $i = m-1$) for domain P_{m-1} can be written as:

$$\frac{p}{\xi_i} r_i^{\theta_i} \tilde{h}_i = \frac{(N_i - 1 - \theta_i)}{r_i} \frac{d\tilde{h}_i}{dr_i} + \frac{d^2\tilde{h}_i}{dr_i^2} - \lambda_{i+1} r_i^{\theta_i} \tilde{h}_i B_{i+1}, \qquad i = m-1. \quad \text{(A33)}$$

The general solution of equation (A33) is:

$$\tilde{h}_i = C_{1i} r_i^{\nu_i E_i} \mathrm{I}_{\nu_i}\left(\gamma_i r_i^{E_i}\right) + C_{2i} r_i^{\nu_i E_i} \mathrm{K}_{\nu_i}\left(\gamma_i r_i^{E_i}\right), \qquad i = m-1, \quad \text{(A34)}$$

where:

$$E_i = (2 + \theta_i)/2, \qquad i = m-1, \quad \text{(A35)}$$

$$\nu_i = 1 - N_i/(2E_i), \qquad i = m-1, \quad \text{(A36)}$$

$$\gamma_i = \sqrt{p/\xi_i + \lambda_{i+1} B_{i+1}}/E_i, \qquad i = m-1. \quad \text{(A37)}$$

By applying the same reasoning as in domain P_m, we assume $\theta_{m-1} > -2$, so the boundary condition (A4, $i = m-1$) implies:

$$C_{2i} = 2C_{1i} \sin(\nu_i \pi)/\pi, \qquad i = m-1, \quad \text{(A38)}$$

$$N_i > n_i - 1, \qquad i = m-1. \quad \text{(A39)}$$

The fracture skin equation (A5, $i = m-1$) gives:

$$C_{1i} = \tilde{h}_{i-1}/A_i, \qquad i = m-1, \quad \text{(A40)}$$

where:

$$A_i = l_i^{\nu_i E_i}\left[\mathrm{I}_{-\nu_i}\left(\gamma_i l_i^{E_i}\right) + l_i^{E_i} \sigma_i \gamma_i E_i \mathrm{I}_{1-\nu_i}\left(\gamma_i l_i^{E_i}\right)\right], \qquad i = m-1, \quad \text{(A41)}$$

which gives:

$$\tilde{h}_i = \tilde{h}_{i-1} r_i^{\nu_i E_i} \mathrm{I}_{-\nu_i}\left(\gamma_i r_i^{E_i}\right)/A_i, \qquad i = m-1. \quad \text{(A42)}$$

For substituting in the exchange term of domain P_{m-2}, we obtain:

$$\left(d\tilde{h}_i/dr_i\right)_{r_i=l_i} = \tilde{h}_{i-1} B_i, \qquad i = m-1, \quad \text{(A43)}$$

where:

$$B_i = \bar{A}_i/A_i, \qquad i = m-1, \quad \text{(A44)}$$

$$\bar{A}_i = l_i^{\nu_i E_i + E_i - 1} \gamma_i E_i \mathrm{I}_{1-\nu_i}\left(\gamma_i l_i^{E_i}\right), \qquad i = m-1. \quad \text{(A45)}$$

[59] Applying the same reasoning for domain P_i, $1 < i < m-1$ as for domain P_{m-1}, but with boundary conditions (A4, $1 < i < m-1$) and fracture skin equation (A5, $1 < i < m-1$), we obtain the following by recurrence, using $i = m-2, \ldots, 2$, for $\theta_i > -2$ and $N_i > n_i - 1$:

$$\tilde{h}_i = \tilde{h}_{i-1} r_i^{\nu_i E_i} \mathrm{I}_{-\nu_i}\left(\gamma_i r_i^{E_i}\right)/A_i, \qquad i = 2, \ldots m-2, \quad \text{(A46)}$$

$$\left(d\tilde{h}_i/dr_i\right)_{r_i=l_i} = \tilde{h}_{i-1} B_i, \qquad i = 2, \ldots, m-2, \quad \text{(A47)}$$

where:

$$A_i = l_i^{\nu_i E_i}\left[\mathrm{I}_{-\nu_i}\left(\gamma_i l_i^{E_i}\right) + l_i^{E_i} \sigma_i \gamma_i E_i \mathrm{I}_{1-\nu_i}\left(\gamma_i l_i^{E_i}\right)\right], \quad i = 2, \ldots, m-2, \quad \text{(A48)}$$

$$B_i = \bar{A}_i/A_i, \qquad i = 2, \ldots, m-2, \quad \text{(A49)}$$

$$\bar{A}_i = l_i^{\nu_i E_i + E_i - 1} \gamma_i E_i \mathrm{I}_{1-\nu_i}\left(\gamma_i l_i^{E_i}\right), \qquad i = 2, \ldots, m-2, \quad \text{(A50)}$$

and:

$$E_i = (2 + \theta_i)/2, \qquad i = 2, \ldots, m-2, \quad \text{(A51)}$$

$$\nu_i = 1 - N_i/(2E_i), \qquad i = 2, \ldots, m-2, \quad \text{(A52)}$$

$$\gamma_i = \sqrt{p/\xi_i + \lambda_{i+1} B_{i+1}}/E_i, \qquad i = 2, \ldots, m-2. \quad \text{(A53)}$$

[60] For domain P_1, with equation (A47, $i = 2$), the diffusion equation (A1, $i = 1$) can be written as:

$$\frac{p}{\xi_1} r_1^{\theta_1} \tilde{h}_1 = \frac{(N_1 - 1 - \theta_1)}{r_1} \frac{d\tilde{h}_1}{dr_1} + \frac{d^2\tilde{h}_1}{dr_1^2} - \lambda_2 r_1^{\theta_1} \tilde{h}_1 B_2. \quad \text{(A54)}$$

The general solution of equation (A54) is:

$$\tilde{h}_1 = C_{11} r_1^{\nu_1 E_1} \mathrm{I}_{\nu_1}\left(\gamma_1 r_1^{E_1}\right) + C_{21} r_1^{\nu_1 E_1} \mathrm{K}_{\nu_1}\left(\gamma_1 r_1^{E_1}\right). \quad \text{(A55)}$$

The boundary condition (A3) implies:

$$C_{11} = 0. \tag{A56}$$

Using equation (A13), we obtain:

$$d\tilde{h}_1/dr_1 = -C_{21}\gamma_1 E_1 r_1^{\nu_1 E_1 + E_1 - 1}\mathrm{K}_{\nu_1 - 1}\left(\gamma_1 r_1^{E_1}\right). \tag{A57}$$

With equation (A57) and the pumping chamber skin equation (A7), we obtain:

$$C_{21} = \tilde{h}_w / A_1, \tag{A58}$$

$$\tilde{h}_1 = \tilde{h}_w r_1^{\nu_1 E_1}\mathrm{K}_{\nu_1}\left(\gamma_1 r_1^{E_1}\right)/A_1, \tag{A59}$$

where:

$$A_1 = l_1^{\nu_1 E_1}\left(\mathrm{K}_{\nu_1}\left(\gamma_1 l_1^{E_1}\right) + r_w\sigma_w\gamma_1 E_1 l_1^{E_1 - 1}\mathrm{K}_{\nu_1 - 1}\left(\gamma_1 l_1^{E_1}\right)\right). \tag{A60}$$

For substituting into the exchange term of the pumping well:

$$\left(d\tilde{h}_1/dr_1\right)_{r_1 = r_w} = -\tilde{h}_w r_w^{\nu_1 E_1 + E_1 - 1}\gamma_1 E_1 \mathrm{K}_{\nu_1 - 1}\left(\gamma_1 r_w^{E_1}\right)/A_1. \tag{A61}$$

[61] Using equation (A61) and the pumping chamber mass balance differential equation (A6), we obtain the drawdown for the pumping well:

$$\tilde{h}_w = QA_1/[p(pS_wA_1 + \bar{A}_1)] \tag{A62}$$

where:

$$\bar{A}_1 = \mathrm{G}_{n_1}(b_1)K_1 r_w^{N_1/2}\gamma_1 E_1 \mathrm{K}_{\nu_1 - 1}\left(\gamma_1 r_w^{E_1}\right) \tag{A63}$$

Appendix B: Consistency of Solutions

[62] In the drawdown solutions (equations (23), (24), (31)), all the quantities are positive except for ν_i, the skin factors and possibly some modified Bessel functions of the first kind with negative order, which could lead to singularities for null denominators and negative square root arguments. Nevertheless, drawdown solutions are always calculable since all Bessel functions arguments are finite:

$$\theta_i > -2 \Longrightarrow E_i > 0 \Longrightarrow \gamma_i > 0 \Longrightarrow 0 \le \gamma_i l_i^{E_i} < +\infty \quad \text{and}\, 0 \le \gamma_i r_i^{E_i} < +\infty$$

and the only term possibly including a modified Bessel function of the second kind with null argument (block centre) is finite. Indeed, for $\nu_i > 0$, and using the reflection formula (A16), this term becomes:

$$r_i^{\nu_i E_i}\mathrm{I}_{-\nu_i}\left(\gamma_i r_i^{E_i}\right) = r_i^{\nu_i E_i}\left(\mathrm{I}_{\nu_i}\left(\gamma_i r_i^{E_i}\right) + 2\sin(\pi\nu_i) \cdot \mathrm{K}_{\nu_i}\left(\gamma_i r_i^{E_i}\right)/\pi\right), \tag{B1}$$

then, for $0 \le \gamma_i r_i^{E_i} \ll \sqrt{\nu_i + 1}$, using the asymptotic behaviors (equations (A18) and (A19)):

$$r_i^{\nu_i E_i}\mathrm{I}_{-\nu_i}\left(\gamma_i r_i^{E_i}\right) \approx \frac{(\gamma_i/2)^{\nu_i}}{\Gamma(\nu_i + 1)} r_i^{2\nu_i E_i} + \frac{2}{\pi}\sin(\pi\nu_i) \cdot \frac{\Gamma(\nu_i)}{2}\left(\frac{\gamma_i}{2}\right)^{-\nu_i} < +\infty. \tag{B2}$$

Thus by recurrence, all drawdown solutions are finite.

[63] In the numerical calculation of equations (23), (24), and (31), Bessel function overflows can be avoided by applying analytical reductions using reflection formulae (equations (A15) and (A16)) and asymptotic behaviors for large arguments:

$$\mathrm{I}_x(Z) \approx \exp(Z)/\sqrt{2\pi Z}, \qquad x \ge 0, \qquad \left|x^2 - 1/4\right| \ll Z, \tag{B3}$$

$$\mathrm{K}_x(Z) \approx \exp(-Z)/\sqrt{\pi/2Z}, \qquad x \ge 0, \qquad \left|x^2 - 1/4\right| \ll Z. \tag{B4}$$

Appendix C: Infinitesimal Source Solution for a Single Porosity

[64] For a single porosity, the infinitesimal source solution is obtained from equation (24) by assuming a null well storage ($S_w = 0$) and taking the well exchange radius r_w as tending to 0. With equation (A15) and:

$$\lim_{Z \to 0}\left(Z^x \mathrm{K}_x(Z)\right) = 2^{x-1}\Gamma(x), \qquad z > 0, \tag{C1}$$

$$D_1 = Qr_1^{\nu_1 E_1}/\left(\mathrm{G}_{n_1}(b_1)K_1 E_1^{1-\nu_1} D_2^{\nu_1/2} 2^{-\nu_1}\Gamma(1 - \nu_1)\right), \tag{C2}$$

$$D_2 = 1/\xi_1 + \lambda_2 B_2/p, \tag{C3}$$

we obtain for a single porosity ($\lambda_2 = 0$):

$$\tilde{h}_1 = D_1 p^{-1-\nu_1/2}\mathrm{K}_{\nu_1}\left(\sqrt{pD_2}r_1^{E_1}/E_1\right). \tag{C4}$$

This can be inverted analytically using:

$$\mathrm{L}\left[\frac{1}{2}\left(\frac{Z}{2}\right)^x \Gamma\left(-x, \frac{Z^2}{4t}\right)\right] = p^{-1-x/2}\mathrm{K}_x\left(Z\sqrt{p}\right), \tag{C5}$$

where $\Gamma(x, Z)$ is the complementary incomplete gamma function, which gives:

$$h_1 = Qr_1^{2\nu_1 E_1}\Gamma\left(-\nu_1, r_1^{2E_1}/4E_1^2\xi_1 t\right)/\left(4\pi^{n_1/2} b_1^{3-n_1} K_1 E_1 \Gamma(N_1/2E_1)/ \cdot \Gamma(N_1/2)\right) \tag{C6}$$

in which we usually assume $n_1 = N_1$ without loss of generality, as stated in the discussion. Note that deriving the infinitesimal source solution from a dimensionless finite source solution is not possible because the dimensionless radius r_1/r_w tends to infinity.

[65] At any given distance r_1 from the well, two distinct models $h_1(N_1, \theta_1, K_1, S_{s1})$ and $\bar{h}_1(\bar{N}_1, \bar{\theta}_1, \bar{K}_1, \bar{S}_{s1})$ with the same flow dimension ($N'_1 = \bar{N}'_1$, $\nu_1 = \bar{\nu}_1$) have the same transient drawdown $h_1(r_1, t) = \bar{h}_1(r_1, t)$ for:

$$\bar{K}_1 = K_1 \mathrm{f}\left(\bar{N}_1, \bar{\theta}_1\right)/\mathrm{f}(N_1, \theta_1), \tag{C7}$$

$$\bar{S}_{s1} = \frac{\bar{K}_1}{r_1^{2(\bar{E}_1 - E_1)}\xi_1}\left(\frac{\bar{E}_1}{E_1}\right)^2, \tag{C8}$$

where:

$$\mathrm{f}(N_1, \theta_1) = r_1^{2\nu_1 E_1}/\left(\pi^{N_1/2} b^{3-N_1} E_1 \Gamma(N_1/2E_1)/\Gamma(N_1/2)\right). \tag{C9}$$

Notation

Subscripts

- c Critical
- C Cubic
- f Fractal scaling
- i, j Porosity domain index
- ℓ Laminar
- m Number of porosity domains
- s Specific
- S Spherical
- t Turbulent
- w Pumping well

Variables and functions

- A_i Truncated block exchange area, m^2
- b_i Orthoradial length, m
- c_i Total compressibility, m s^2 kg^{-1}
- D_i Truncated block density, m^{-3}
- e_i Fracture aperture of domains $P_{i<m}$, m
- G Unit-radius hyperspherical block or pumping chamber area function
- h_i Drawdown in domains $P_{i=w,1,\ldots,m}$, m
- H Heaviside function
- I_x Modified Bessel function of the first kind and order x
- k_i Fractal permeability, $m^{2\,+\,\theta_i}$
- K_{fi} Hydraulic conductivity, m s^{-1}
- K_i Hydraulic conductivity on a unit-radius hypersphere, $m^{1-N_i+n_i+\theta_i}$ s^{-1}
- K_x Modified Bessel function of the second kind and order x
- l_1 r_w, m
- l_i Hyperspherical block radius of domains $P_{i>1}$, m
- $\bar{l}_i$ Hypercubic block half-thickness of domains $P_{i>1}$, m
- L Laplace transform
- m Number of porosity domains, −
- n_1 Euclidean limit dimension of domain P_1 and pumping chamber shape dimension, −
- n_i Block shape dimension of domains $P_{i>1}$, −
- N_i Fractal density dimension, −
- N'_i Flow or spectral dimension, −
- p_w Pumping chamber nonlinear head loss exponent, −
- p Laplace variable
- P_i Porosity domain i, −
- Q Injection flow rate, negative for pumping, m^3 s^{-1}
- Q_c Critical flow rate, m^3 s^{-1}
- q_i Exchange flow rate density between $P_{i<m}$ and P_{i+1}, s^{-1}
- r_1 Radial Euclidean distance from the source center, m
- r_i Radial Euclidean distance from the symmetry centre of blocks embedding $P_{i>1}$, m
- r_w Pumping well exchange radius, m
- S_{sfi} Specific storage, m^{-1}
- S_{si} Specific storage on a unit-radius hypersphere, $m^{1-N_i+n_i}$
- S_w Pumping well capacity, m^2
- t Time elapsed from start of pump test, s
- V_i Truncated block volume, m^3
- α_n $2\pi^{n/2}/\Gamma(n/2)$
- β_i Correction factors for block radius $l_{i>1}$, −
- Γ Gamma function.
- Δ_i Volume density of blocks $P_{i>1}$, −
- θ_i Anomalous diffusion exponent, −
- θ'_i Random walk dimension, −
- λ_{i+1} Exchange coefficient between $P_{i\,<\,m}$ and P_{i+1}, $m^{N_i\,-\,n_i\,-\,\theta_i\,-\,1}$
- Λ_i Exchange area density of blocks embedding $P_{i>1}$, m^{-1}
- μ Fluid dynamic viscosity, m^{-1} s^{-1} kg
- τ_i Effective fracture volume ratio, −
- ξ_i Diffusivity on a unit radius hypersphere, $m^{2+\theta_i}$ s^{-1}
- $\bar{\rho}$ Fluid voluminal weight, kg m^{-2} s^{-2}
- σ_1 σ_w, −
- σ_i Fracture skin factor between $P_{i\,>\,1}$ and $P_{i\,-\,1}$
- σ_w Pumping chamber skin factor, −
- $\sigma_{w\ell}$ Pumping chamber linear (laminar) skin factor, −
- σ_{wt} Pumping chamber nonlinear (turbulent) skin factor, $m^{3(1-p_w)}$ s^{p_w-1}
- ϕ_{fi} Fracture fractal density or porosity, −
- ϕ_i Fracture fractal density or porosity on a unit radius hypersphere, $m^{n_i-N_i}$
- χ_i Exchange area density between $P_{i>1}$ and P_{i-1}, m^{-1}

[66] **Acknowledgments.** The authors wish to thank the reviewers, Rajagopal Raghavan, and anonymous for their helpful comments.

References

Abdassah, D., and I. Ershaghi (1986), Triple-porosity systems for representing naturally fractured reservoirs, *SPE Form. Eval. Trans. AIME*, *284*, 113–127.

Acuna, J. A., and Y. C. Yortsos (1995), Application of fractal geometry to the study of networks of fractures and their pressure transient, *Water Resour. Res.*, *31*(3), 527–540.

Bai, M., D. Elsworth, and J.-C. Roegiers (1993), Multiporosity/multipermeability approach to the simulation of naturally fractured reservoirs, *Water Resour. Res.*, *29*(6), 1621–1633.

Barenblatt, G. R., I. P. Zheltov, and I. N. Kochina (1960), Basic concepts in the theory of seapage of homogeneous liquids in fractured rocks, *J. Appl. Math. Mech. Eng. Transl.*, *24*(5), 1286–1303.

Barker, J. A. (1985a), Generalized well function evaluation for homogeneous and fissured aquifers, *J. Hydrol.*, *76*, 143–154.

Barker, J. A. (1985b), Block-geometry functions characterizing transport in densely fissured media, *J. Hydrol.*, *77*, 263–279.

Barker, J. A. (1988), A generalized radial flow model for hydraulic tests in fractured rock, *Water Resour. Res.*, *24*(10), 1796–1804.

Barton, C. C., and P. A. Hsieh (1989), *Physical and Hydrological-Flow Properties of Fractures*, Guidebook T385, AGU, Las Vegas, Nev.

Bernard, S., F. Delay, and G. Porel (2006), A new method of data inversion for the identification of fractal characteristics and homogenization scale from hydraulic pumping tests in fractured aquifers, *J. Hydrol.*, *328*(3–4), 647–658.

Boulton, N. S., and T. D. Streltsova (1977), Unsteady flow to a pumped well in a fissured water-bearing formation, *J. Hydrol.*, *35*, 257–269.

Bourdet, D., J. A. Ayoub, T. M. Whittle, Y. M. Pirard, and V. Kniazeff (1983), Interpreting well tests in fractured reservoirs, *World Oil*, *1975*, 77–87.

Camacho-Velázquez, R., M. Vásquez-Cruz, R. Castrejón-Aivar, and V. Arana-Ortiz (2005), Pressure-transient and decline-curve behaviors in naturally fractured vuggy carbonate reservoirs, *SPE Reservoir Eval. Eng.*, *8*(2), 95–112.

Chang, J., and Y. C. Yortsos (1990), Pressure-transient analysis of fractal reservoirs, *SPE Form. Eval.*, *5*, 31–38.

Chelidze, T., and Y. Gueguen (1990), Evidence of fractal fracture, *Int. J. Rock Mech. Miner. Sci. Geomech. Abstr.*, *27*(3), 223–225.

Closmann, P. J. (1975), An aquifer model for fissured reservoirs, *SPE J.*, *15*(5), 385–398.

de Dreuzy, J.-R., and P. Davy (2007), Relation between fractional flow models and fractal or long-range 2-D permeability fields, *Water Resour. Res.*, *43*, WO4431, doi:10.1029/2006WR005236.

Delay, F., A. Kaczmaryk, and P. Ackerer (2007), Inversion of interference hydraulic pumping tests in both homogeneous and fractal dual media, *Adv. Water Resour.*, *30*(3), 314–334.

Hamm, S.-Y., and P. Bidaux (1996), Dual-porosity fractal models for transient flow analysis in fractured rocks, *Water Resour. Res.*, *32*(9), 2733–2745.

Havlin, S., and D. Ben-Avraham (1987), Diffusion in disordered media, *Adv. Phys.*, *36*, 695–798.

Le Borgne, T., O. Bour, J. R. de Dreuzy, P. Davy, and F. Touchard (2004), Equivalent mean flow models for fractured aquifers: Insights from a pumping tests scaling interpretation, *Water Resour. Res.*, *40*(3), W03512, doi:10.1029/2003WR002436.

Liu, J. C., G. S. Bodvarsson, and Y. S. Wu (2003), Analysis of flow behavior in fractured lithophysal reservoirs, *J. Contam. Hydrol.*, *62–63*, 189–211.

Lods, G., and P. Gouze (2004), WTFM, software for well test analysis in fractured media combining fractional flow with double porosity and leakance, *Comput. Geosci.*, *30*, 937–947.

Mandelbrot, B. B. (1983), *The Fractal Geometry of Nature*, 468 pp., W.H. Freeman, New York.

Moench, A. F. (1984), Double porosity models for a fractured groundwater reservoir with fracture skin, *Water Resour. Res.*, *20*(7), 831–846.

Nolte, D. D., L. J. Pyrak-Nolte, and N. G. M. Cook (1989), The fractal geometry of flow paths in natural fractures in rock and the approach to percolation, *Pure Appl. Geophys.*, *131*, 111–138.

O'Shaughnessy, B., and I. Procaccia (1985), Diffusion on fractals, *Phys. Rev. A*, *32*(4), 3073–3083.

Papadopulos, I. S., and H. H. Cooper Jr. (1967), Drawdown in a well of large diameter, *Water Resour. Res.*, *3*(1), 241–244.

Pulido, H., F. Samaniego, J. Rivera, F. Diaz, and G. Galicia (2006), Well test analysis for naturally fractured reservoirs with transient interporosity matrix, microfractures, and fractures flow, in *Proceedings of the Thirty-First Workshop on Geothermal Reservoir Engineering*, Stanford Univ., Calif., Jan. 30–Feb. 1, SGP-TR-179.

Pulido, H., F. Samaniego, H. Cinco-Ley, J. Rivera, F. Diaz, and G. Galicia (2007), Triple-porosity model-dual permeability with transient hydraulic diffusivity in naturally frectured reservoirs, in *Proceedings of the Thirty-Second Workshop on Geothermal Reservoir Engineering*, Stanford Univ., Calif., Jan. 22–24, SGP-TR-183.

Rodriguez, F., V. Arana-Ortiz, and H. Cinco-Ley (2004), Well test characterization of small and large scale secondary porosity in naturally fractured reservoirs, *SPE 90287*, Annual technical conference and exhibition, Houston Texas, USA, Sept. 26–29.

Rorabaugh, M. J. (1953), Graphical and theoretical analysis of step-drawdown test of artesian well, *Proc. Am. Soc. Civil Eng.*, *79*(362), 23pp.

Sahimi, M., M. C. Robertson, and C. G. Sammis (1993), Fractal distribution of earthquake hypocenters and its relation to fault patterns and percolation, *Phys. Rev. Lett.*, *70*(14), 2186–2189.

Stehfest, H. (1970), Numerical inversion of Laplace transforms, *Commun. ACM*, *13*(1), 47–49.

Theis, C. V. (1935), The relation between the lowering of the piezometric surface and the rate and duration of discharge of a well using ground water storage, *Trans. AGU*, *16*, 519–526.

Turcotte, D. L. (1986), Fractals and fragmentation, *J. Geophys. Res*, *91*(B2), 1921–1926.

van Everdingen, A. F. (1953), The skin effect and its influence on the productive capacity of a well, *Trans. AIME*, *198*, 171–176.

Walker, D., and R. Roberts (2003), Flow dimensions corresponding to hydrogeologic conditions, *Water Resour. Res.*, *39*(12), 1349, doi:10.1029/2002WR001511.

Warren, J. E., and P. J. Root (1963), The behaviour of naturally fractured reservoirs, *SPE J.*, *3*(2), 245–255.

P. Gouze and G. Lods, Laboratoire Géosciences, Université Montpellier 2 - CNRS, Subsurface, Pl. Bataillon, 34095 Montpellier Cedex 5, France. (gouze@msem.univ-montp2.fr; lods@msem.univ-montp2.fr)